CHEMICAL REVIEWS

REVIEW

pubs.acs.org/CR

Review and Analysis of Molecular Simulations of Methane, Hydrogen, and Acetylene Storage in Metal−Organic Frameworks

Rachel B. Getman,† Youn-Sang Bae, Christopher E. Wilmer, and Randall Q. Snurr*

Department of Chemical and Biological Engineering, Northwestern University, Evanston, Illinois 60208, United States

CONTENTS

1. Introduction 703
2. Simulation Methods 704
   2.1. The Model 704
   2.2. Force Field Potentials and Parameters 704
   2.3. Simulating Gas Adsorption with Grand Canonical Monte Carlo 705
   2.4. Quantum Chemical Calculations 706
3. Gas Storage in MOFs without Strongly Binding Sites 706
   3.1. Optimal Design Characteristics Revealed by Simulation 707
      3.1.1. CH_4 Storage 707
      3.1.2. H_2 Storage 708
   3.2. Comparison of Simulated Adsorption Isotherms with Experiment for MOFs and COFs without Strongly Binding Sites 709
      3.2.1. CH_4 Storage 709
      3.2.2. H_2 Storage 710
   3.3. Acetylene Storage 711
4. Adsorption in MOFs with Open Metal Sites in the Nodes 712
   4.1. H_2 Interactions with Open Metal Sites 712
   4.2. Methane Adsorption in M-MOF-74 712
   4.3. Special Considerations for Calculating Gas Molecule Interactions at Open Metal Sites 712
5. Simulating Hydrogen Adsorption in MOFs with Cation Sites on the Linkers 713
   5.1. Doped MOFs 713
   5.2. Functionalized MOFs 714
   5.3. How Simulation Methods Impact Gas Adsorption Results 715
      5.3.1. Effect of Interaction Model on Calculated H_2 Adsorption Uptake 715
      5.3.2. Limitations of Pair Potential Models 717
   5.4. Challenges in Force Field Development 717
6. Calculating Heats of Adsorption 718
7. Using Simulations to Guide Experiment 719
8. Conclusions and Outlook 719
Associated Content 720
Author Information 720
Biographies 720
Acknowledgment 721
References 721

1. INTRODUCTION

Gas adsorption in metal−organic frameworks (MOFs) has been one of the most actively studied applications of this new and exciting class of materials. Applications of adsorption in MOFs include chemical separations, sensing, and gas storage. As discussed throughout this issue, MOFs are porous, crystalline materials that comprise metal or metal oxide "nodes" connected by organic "linker" compounds.[1] Some of the most studied MOFs are shown in Figure 1. MOFs have large internal surface areas, which make them attractive for gas adsorption. Additionally, they are synthesized in a modular fashion and are thus tunable: one can assemble different combinations of metal nodes and organic linkers to obtain a large variety of unique materials with different affinities for different gases. MOFs with surface areas over 6000 m^2/g have been synthesized to date,[2,3] and these have exhibited exceptional gas uptake.

Gas molecules typically physisorb to MOF surfaces, interacting with framework atoms through dispersive and repulsive interactions. Many researchers have sought to improve gas storage in MOFs by tuning gas molecule interactions with the frameworks. This can be done through catenation of multiple frameworks,[4−9] inclusion of unsaturated "open" metal sites in the nodes,[10−12] and incorporation of various functional groups (including metal cation sites) in the organic linkers.[13,14] The ability to introduce the appropriate features for specific applications, along with the huge variety of potential MOF structures, opens up the possibility to truly design MOFs for desired applications.

In this work, we review computational studies of gas adsorption in MOFs, focusing on molecular modeling of methane, hydrogen, and acetylene. People are interested in storing these gases for the following reasons:

- Methane is a desirable fuel because it burns more cleanly than gasoline and has a higher hydrogen to carbon (H/C) ratio than any other hydrocarbon fuel.[15] However, a major drawback is that the volumetric energy density of compressed methane is only one-third that of gasoline.[15] Materials that increase the volumetric density of stored methane could help expand the role of natural gas (which is mostly methane) as a transportation fuel. To motivate research and development of methane storage materials, the Department of Energy (DOE) has set storage targets of 180 v(STP)/v, i.e., 180 STP (standard temperature and pressure) liters of CH_4 stored per liter of storage vessel. MOFs have already been synthesized that exceed this value (see, e.g., refs 16 and 17).

Special Issue: 2012 Metal-Organic Frameworks

Received: June 13, 2011
Published: December 21, 2011

dx.doi.org/10.1021/cr200217c | *Chem. Rev.* 2012, 112, 703–723

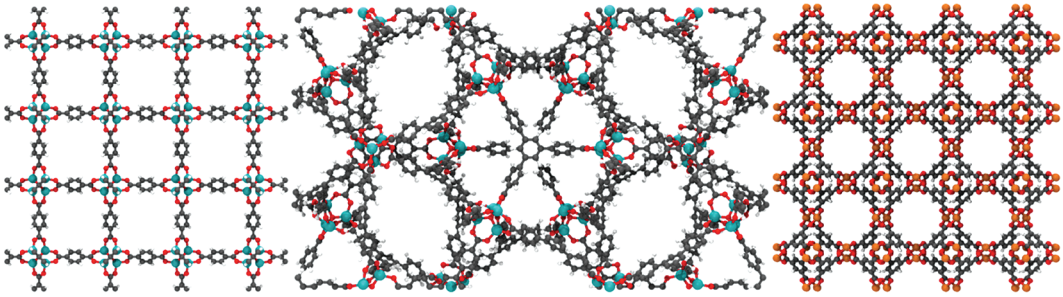

Figure 1. Three common metal−organic frameworks investigated for their gas storage properties: IRMOF-1 (left), MOF-177 (middle), and HKUST-1 (right).

- Hydrogen is an attractive fuel because it has a high gravimetric energy density, it is nontoxic, and its oxidation product is water. However, the very small volumetric density of H_2, 0.0899 kg/m^3 at STP, makes storage difficult and is a major hurdle for the expansion of the hydrogen economy. The DOE has established targets for hydrogen storage systems of 2.5 kWh/kg and 2.3 kWh/L, which translate into 7.0 wt % H_2 and 70 g H_2/L for an entire H_2 storage system.[18] Short-term targets are 5.2 wt % H_2 and 40 g H_2/L at a minimum temperature of −30 °C and a maximum pressure of 100 bar by 2015. No material has yet been synthesized that meets these criteria, although computational studies of H_2 in MOFs have proposed design strategies that could meet the 2015 gravimetric targets (see, e.g., refs 19 and 20).
- Acetylene is one of the major building blocks of organic chemistry, and 400 000 tonnes are produced annually worldwide today.[21] However, transportation of acetylene is difficult because, unlike CH_4 and H_2, acetylene storage is limited to <2 atm in order not to cross an explosive threshold. This has spurred interest in high surface area materials that can store acetylene without the need for high pressure.

Molecular simulation is becoming an indispensible tool for MOF design. Simulations can provide molecular level details of chemical phenomena that cannot be viewed directly in experiments. Additionally, it is usually much simpler to construct a MOF model on the computer than it is to synthesize and characterize the material in the lab. Therefore, one can probe a large number of materials via simulation more easily than through experiment. Taking advantage of these features can accelerate the generation of new insights. Simulations have been used to assess the capabilities of MOFs,[8,22−26] screen MOF design features before synthesis,[19,25] and predict new MOF structures.[2] Simulations are also useful for predicting uptake at high temperatures and pressures, which are difficult to achieve experimentally. This is particularly useful for assessing MOFs for gas storage applications, as the desired storage conditions are typically at high pressure. There have thus been many computational studies of gas storage in MOFs and other porous materials, as discussed in prior reviews.[9,22,23,25]

In this review, we discuss and analyze recent computational studies of adsorption of methane, hydrogen, and acetylene in porous materials and show how simulation has been used to guide the design of these materials for gas storage. We additionally discuss the state-of-the-art in simulation techniques and the challenges associated with performing molecular simulations of gas molecules in MOFs. Throughout the review, we highlight both the successes and limitations of such simulations. The paper is organized as follows: section 2 discusses models and methods commonly used to calculate gas adsorption in MOFs. Section 3 discusses how these models and methods have been used to assess and design MOFs for CH_4, H_2, and C_2H_2 storage. Sections 4 and 5 discuss gas adsorption at open metal sites in the nodes and linkers, respectively, the different computational strategies required to calculate adsorbate interactions at these sites, and the challenges associated with performing such calculations. Section 6 discusses how simulations can be used to calculate the average enthalpy of adsorption, which is a useful quantity for assessing uptake capabilities. Section 7 discusses specific examples where simulations have been used to guide experiments.

2. SIMULATION METHODS

2.1. The Model

Gas molecules typically physisorb in MOFs through dispersive, repulsive, and Coulombic interactions, and thus details about the electronic structure can often be ignored. (Exceptions to this are when the MOF contains open metal or other strongly binding functional groups that promote chemical bonding. See sections 4 and 5.) In a typical model based on classical mechanics, each atom is modeled as a spherical particle. In some cases, further simplifications can be made; for example, in a so-called "united-atom" model, a small molecule like CH_4 is treated as a single sphere.[27]

Within the all-atom or united-atom models, there is a significant amount of freedom in choosing how the smallest units (atoms or molecules) interact with each other. One needs to choose both the functional form of the interactions (e.g., harmonic, Morse,[28] Lennard-Jones,[29] etc.) and the specific parameters used in the functional form. The combination of a functional form with a particular set of parameters completely describes the interactions in the model, which is often called the force field. The force field describes the potential energy, $\mathcal{V}$, of a particular configuration of atoms.

Specialized force fields have been developed for simulating hydrocarbons,[30] organic molecules,[31] and proteins,[32] as well as for describing particular phenomena, such as charge transport[33] and reactions.[34] The following section describes commonly used force fields in gas adsorption simulations.

2.2. Force Field Potentials and Parameters

For simulating adsorption of small molecules like hydrogen, methane, or acetylene, it is often reasonable to assume that the gas molecules and MOF structure are completely rigid. In this case, there are only intermolecular interactions between nonbonded atoms, which are often modeled via a

dx.doi.org/10.1021/cr200217c |*Chem. Rev.* 2012, 112, 703–723

Lennard-Jones (LJ) + Coulomb potential.

$$\mathscr{V}_{ij}(r_{ij}) = 4\varepsilon_{ij}\left[\left(\frac{\sigma_{ij}}{r_{ij}}\right)^{12} - \left(\frac{\sigma_{ij}}{r_{ij}}\right)^{6}\right] + \frac{q_i q_j}{4\pi\varepsilon_0 {r_{ij}}^2} \quad (1)$$

Here r_{ij} is the separation between atoms i and j having charges q_i and q_j. For nonbonded interactions, pairwise additivity is usually assumed, so that the total energy is the sum of the interaction energy between every pair of atoms. As discussed below, it should be kept in mind that this is an approximation. The Lennard-Jones part of the potential describes attractive van der Waals interactions between pairs of nonbonded atoms, as well as their mutual repulsion at shorter distances. The two Lennard-Jones parameters, ε and σ, are the minimum potential energy and the separation where $\mathscr{V} = 0$, respectively. The form of the Lennard-Jones potential, with repulsive and attractive terms in r^{-12} and r^{-6}, respectively, was chosen because it can reproduce the location of the energy minimum for many nonbonding systems with good accuracy, and it is computationally convenient to calculate r^{-12} if r^{-6} has already been computed. However, other potentials, such as the Morse potential, which includes an exponential term, can be more accurate, especially for stronger interactions. (We discuss the Morse potential in greater detail later.)

The partial charges in the Lennard-Jones plus Coulomb potential account for polarity of the gas molecules (e.g., the quadrupole moment of H_2) and the electric field generated by the framework atoms. Note that sometimes charges are placed on sites off of the atom centers. For example, the Darkrim—Levesque (DL) model[35] for H_2 accounts for the quadrupole moment by placing three partial charges along the H—H axis—a charge of +0.468 on each H nucleus and a charge of −0.936 at the center of mass—in addition to the Lennard-Jones site at the H_2 center of mass. Partial charges for framework atoms are typically obtained from quantum mechanical calculations on small appropriately truncated fragments of the crystal or sometimes on periodic structures. A single-point calculation is performed, followed by determination of the charges. Methods that fit the charges to the electrostatic potential, such as ChelpG,[36] are particularly suited for obtaining charges to be used in molecular simulations. Faster methods to calculate partial charges for framework atoms have been developed recently,[37,38] for example, the charge equilibration method.[38,39]

The force field must include parameters for gas/framework interactions as well as interactions between the gas molecules themselves. The latter are often taken from established force fields in the literature for bulk fluids. For example, one widely used model for H_2 treats each molecule as a single sphere with a Lennard-Jones site at the center of mass. The LJ parameters were obtained empirically based on the second virial coefficient.[40] Simulations of acetylene adsorption in MOFs have used the OPLS force field,[41,42] and simulations of methane have often used the TraPPE force field.[27,43] The names of these force fields give some indication of their scope: OPLS is an acronym for optimized potentials for liquid simulations and TraPPE stands for transferable potentials for phase equilibria. The OPLS intramolecular parameters were derived from ab initio calculations, and the nonbonded interaction parameters were chosen so that Monte Carlo simulations of 34 pure organic liquids reproduced the experimental heats of vaporization and liquid densities. The TraPPE force field was developed to reproduce vapor—liquid coexistence curves for pure components of various classes of molecules. For example, the parameters for alkanes were fit for methane through dodecane.

For framework atoms in MOFs, the Lennard-Jones parameters are usually taken from rather general force fields, especially DREIDING[44] and the universal force field[39] (UFF). The Lennard-Jones parameters in DREIDING were developed by fitting to reproduce crystal structures of organic compounds in known databases.[45] Given LJ parameters for the atoms of gas molecules and the MOF atoms, the LJ parameters for gas/framework interactions are then calculated using standard "mixing rules". For example, the Lorentz—Berthelot mixing rules[46] use an arithmetic average for σ and a geometric average for ε.

It is not always possible to reproduce strong, specific interactions with the Lennard-Jones + Coulomb potential, for example, interactions with MOF open metal sites. Instead of the two-parameter Lennard-Jones potential, a three-parameter Morse potential is sometimes used in such cases,

$$\mathscr{V}_{ij}(r_{ij}) = D_{ij}\left[1 - e^{-\alpha_{ij}(r_{ij} - r^*_{ij})}\right] \quad (2)$$

The Morse model was developed to describe diatomic vibrational spectra and predated the LJ potential but was not as widely adopted in later molecular simulations.[28] In the Morse potential, D and r^* are analogous to ε and σ in the Lennard-Jones potential, and α controls the width of the potential well of interaction. This additional parameter allows the model to more faithfully reproduce strong binding interactions.[47,48] Recently, researchers have used Morse potentials to model H_2 interactions with exposed metal atoms in porous materials.[19,24,49−51] In these cases, the parameters for the Morse potential were fit to reproduce energies obtained from quantum mechanical calculations.

At low temperatures, quantum diffraction effects become important for light molecules such as H_2 and He, and these must be accounted for to obtain accurate adsorption predictions.[52] Quantum diffraction effects can be exactly captured using path integral Monte Carlo (PIMC).[53] Alternatively, Feynman and Hibbs[54] introduced a more computationally efficient but approximate, quasiclassical potential that also significantly mitigates errors induced by incorrectly treating the particles classically. This Feynman—Hibbs (FH) potential,

$$\mathscr{V}^{\mathrm{FH}}_{ij}(r_{ij}) = \mathscr{V}_{ij}(r_{ij}) + \left(\frac{\hbar^2}{24\mu k_{\mathrm{B}} T}\right)\nabla^2 \mathscr{V}_{ij}(r_{ij}) \quad (3)$$

accurately describes equilibrium of low-temperature systems.[52] Here, $\mathscr{V}_{ij}$ is the usual force field energy between atoms i and j as described above, $\hbar$ is Planck's constant divided by 2π, $\mu = m_i m_j / (m_i + m_j)$ is the reduced mass of the interaction, k_{B} is Boltzmann's constant, and T is the temperature. The FH potential has been used to obtain accurate gas adsorption isotherms at low temperatures.[52,55,56]

2.3. Simulating Gas Adsorption with Grand Canonical Monte Carlo

Gas adsorption properties are usually calculated using Monte Carlo methods, which use random moves to sample a statistical mechanical ensemble and determine average quantities such as the equilibrium uptake and enthalpy.[57] For each configuration of the system, the energy is calculated using the chosen force field as described above. Adsorption isotherms are typically calculated using grand canonical Monte Carlo (GCMC) simulations. In this method, an adsorbate phase at constant temperature T, volume V,

dx.doi.org/10.1021/cr200217c |Chem. Rev. 2012, 112, 703–723

and chemical potential μ is allowed to equilibrate with a gas phase (which is not simulated). The number of molecules N in the adsorbate phase is allowed to fluctuate so that the chemical potentials of the two phases are equal.[58] During the GCMC simulation, adsorbate molecules are subjected to a variety of random moves, such as translation and rotation, insertion of a new molecule into a random position within the system, and deletion of an existing molecule from the system.[46] The moves are accepted or rejected based on the change in potential energy, the specified temperature, and the chemical potential.[46,59] The chemical potential can be related to the pressure of the gas phase using an equation of state. The adsorption uptake is calculated as the average number of molecules N in the adsorbate phase during the simulation.

2.4. Quantum Chemical Calculations

The general models discussed above perform well for predicting gas adsorption in materials without strong binding sites (such as open metal sites). However, as we will show in sections 4 and 5, they are not sufficient for describing strong gas/framework interactions. Quantum chemical methods are typically used to capture these interactions. There are many challenges associated with performing such calculations. The goal is always to balance the accuracy and efficiency of the calculations, which are controlled by several factors, such as the method used for treating electron correlation, the size of the basis set, and which atoms in the MOF are treated quantum chemically. For example, the treatment of electron correlation can significantly impact both computational accuracy and expense. The MP2 method, which is a post-Hartree−Fock method that includes electron correlation perturbatively to second order, provides a good balance between computational accuracy and expense for many systems. In particular, the resolution of identities variation of MP2, RI-MP2, developed by Ahlrichs and co-workers, was optimized for computational efficiency by neglecting long-range correlation and simplifying the four electron terms in the Hartree−Fock solution, and it has been shown to give results in line with MP2 for many molecules.[60] However, MP2 itself can give unreliable results in highly magnetic and radical systems that exhibit significant spin contamination,[61] including some transition metal-containing systems. Additionally, as discussed below, MP2 is not suitable for describing multibody interactions, which can be significant for some systems.[62] The spin-component-scaled implementation of MP2 by Grimme, which separately scales the antiparallel and parallel contributions to the correlation energy, addresses these failings in part with virtually no increase in computational expense.[63]

Many researchers use some form of density functional theory (DFT) instead of MP2 or a higher level of theory to save time. DFT methods write the electron correlation in terms of the electron density, thus reducing a many-dimensional problem to a three-dimensional one and reducing the time necessary to calculate the electronic structure. However, since the actual functional form of the electron correlation is not known, DFT methods are not always accurate, and they generally do not describe weak interactions such as dispersion well. This is discussed in more detail in section 4.3.

Whatever electron correlation method is chosen, it should be carefully selected to ensure computational accuracy. In terms of computational accuracy, common electron correlation methods follow the order DFT < MP2 < coupled cluster (CC) < higher-order methods.[61] Coupled cluster methods use single, double, and/or triple excitation determinants to compute electron correlation. Although CC calculations are more accurate than MP2 and DFT and avoid spin contamination problems, they are also much more computationally demanding. The CCSD(T) method, which includes single and double excitations to infinite order and introduces triple excitations perturbatively, is currently the highest accuracy method that can be routinely applied, but it is still too computationally demanding for many systems involving transition metals.

The chosen basis set also affects the time needed to complete quantum mechanical calculations. Large basis sets including diffuse and polarization functions usually provide more accurate results, but they add to computational expense. Smaller basis sets often require attention to basis set superposition errors (BSSE), i.e. the unphysical tendency of fragments in an interacting supermolecule to "borrow" basis functions from each other to optimize the wave function. One method for minimizing these errors is to apply counterpoise corrections,[64] which estimate the BSSE by calculating the total energy of the supermolecule and the energies of the individual fragments using supermolecule-centered and fragment-centered basis sets. While necessary in some systems, this method increases the computational time.

Finally, the model system used in the quantum chemical calculations can have significant effects on adsorbate/adsorbent binding energies. To date, most binding energies have been calculated on MOF fragments because calculations on periodic structures are too computationally demanding for any electron correlation method other than DFT. We show in section 5 that the size of the MOF fragment used can significantly impact the quantum chemical results.

3. GAS STORAGE IN MOFS WITHOUT STRONGLY BINDING SITES

Although quantum chemical methods are necessary for modeling gas adsorption in MOFs with strongly binding sites, gas adsorption in many MOFs has been successfully calculated using the simple Lennard-Jones + Coulomb models described above. In this section, we highlight studies of methane, hydrogen, and acetylene adsorption in MOFs without strongly binding sites, focusing on reports that have used simulation to guide material design.

There are several ways of reporting adsorption data. First, one may consider the amount adsorbed per unit mass of adsorbent (gravimetric) or the amount adsorbed per unit volume (volumetric). Both gravimetric and volumetric quantities are important for on-board storage of natural gas or hydrogen in vehicles. In addition, simulations yield the total amount adsorbed (also called the absolute adsorption, N_{abs}), but experiments generally measure the so-called excess amount adsorbed (N_{ex}), i.e., the amount adsorbed above what would be present in the absence of the adsorbent. These quantities are related to each other by

$$N_{ex} = N_{abs} - V_g \rho_g \quad (4)$$

where V_g is the pore volume of the adsorbent and ρ_g is the density of the bulk gas phase, which can be calculated using an equation of state. For storage applications, it is the total amount adsorbed (either gravimetric or volumetric) that is of main importance, rather than the excess amount. Finally, one may distinguish between the absolute adsorption and the deliverable capacity. The deliverable capacity is the difference between the amount

adsorbed at the pressure when a gas tank is filled and the amount adsorbed at the delivery pressure (typically ~2 bar).

3.1. Optimal Design Characteristics Revealed by Simulation

3.1.1. CH_4 Storage. There have been several computational studies to investigate desired characteristics of an optimal adsorbent for methane storage. In one of the early simulation studies in MOFs, Düren et al.[65] studied CH_4 adsorption in 18 different materials, including isoreticular MOFs (IRMOFs), molecular squares, zeolites, MCM-41, and carbon nanotubes, to uncover the complex interplay of the factors influencing CH_4 adsorption, especially the surface area, free volume, strength of the energetic interaction, and pore size distribution. They concluded that an ideal material for CH_4 adsorption should have not only a large surface area but also a high free volume, a low framework density, and strong CH_4/adsorbent interactions. They also mentioned that changing one of these parameters might worsen the others and therefore decrease the CH_4 uptake. On the basis of this analysis, they proposed new, not yet synthesized IRMOF materials by replacing or adding atoms in the linker molecules of IRMOF-1. Replacing the hydrogen atoms by bromine atoms (i.e., using 1,4-tetrabromobenzene dicarboxylate as linker molecules; IRMOF-992) introduces stronger interaction sites. The predicted isotherm for IRMOF-992 indeed showed a higher volumetric CH_4 uptake over the whole pressure range, with an average enthalpy (isosteric heat) of adsorption (Q_{st}) at low loading of 14.5 kJ/mol, compared to 10.6 kJ/mol for IRMOF-1. However, due to the higher crystal density, the gravimetric CH_4 uptake was lower than for the other IRMOFs. Using 9,10-anthracenedicarboxylate as the linker molecule (IRMOF-993) resulted in a material with a smaller pore size (6.3 Å) and a significantly reduced surface area (Figure 2a). Nevertheless, the gravimetric and volumetric CH_4 uptake was higher over the whole pressure range. At 35 bar, IRMOF-993 was even predicted to exceed the DOE target value of 180 v(STP)/v. Düren et al. attributed this to an increased number of carbon atoms on the linker compared to the 1,4-benzenedicarboxylate linker in IRMOF-1 as well as to the constricted pore size. They suggested that the Q_{st} of CH_4 increased from 10.6 to 15.5 kJ/mol because of these features. Ma et al.[66] tried to synthesize IRMOF-993 using the proposed linker, but the resulting structure (PCN-13) had a different topology due to the distorted $Zn_4O(CO_2)_6$ motif and showed very limited CH_4 uptake. Building on the idea of synthesizing MOFs having linkers with an increased number of carbon atoms and attempting to increase the pore size, they synthesized a new microporous MOF, PCN-14, by adopting a new ligand, 5,5′-(9,10-anthracenediyl)diisophthalate (Figure 2b). PCN-14 exhibited an absolute CH_4 uptake of 230 v(STP)/v at 35 bar and 290 K (28% higher than the DOE target of 180 v(STP)/v at ambient temperatures) and a heat of adsorption for CH_4 of ~30 kJ/mol, both record highs for methane storage materials.

Düren and Snurr[67] studied CH_4 adsorption in a series of IRMOFs (IRMOF-1, -8, -10, -14, -16) to investigate the effect of the organic linker. As the length of the organic linker increased, the pore size and the pore volume became larger. For pressures up to 40 bar, the calculated CH_4 uptakes in the five IRMOFs did not follow the order of pore volume. This was because the CH_4 isotherms were still far from saturation even at 40 bar. Analyzing their results, we find that, in the low pressure range (<40 bar), the CH_4 uptake increases with increasing number of carbon atoms on the linker. This agrees with the results above for IRMOF-993 and PCN-14.

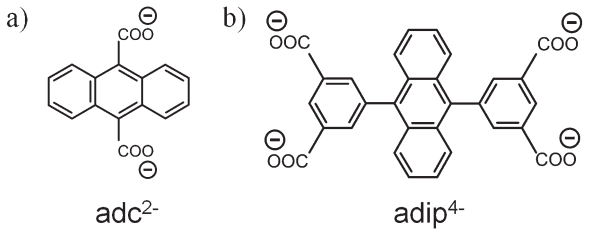

Figure 2. Carboxylate linkers used in (a) IRMOF-993 (and PCN-13) and (b) PCN-14. Reprinted with permission from ref 66. Copyright 2008 American Chemical Society.

Wang[68] did a systematic simulation study on CH_4 adsorption in a series of 10 MOFs with different topologies, including 5 IRMOFs (IRMOF-1, -6, -8, -10, and -14), HKUST-1, 2 coordination polymers with pillared layer structures (CPL-28 and CPL-522), and $Cu(AF_6)(bpy)_2$ (A = Si and Ge). From GCMC simulations for pressures up to 100 bar at 298 K, he investigated the desired characteristics of an optimal adsorbent for CH_4 storage and concluded that the CH_4 uptake at high pressures has a strong correlation with the surface area and free volume.

Gallo and Glossman-Mitnik[69] calculated adsorption isotherms for CH_4 in two large-surface-area MOFs (IRMOF-1 and MOF-177), two catenated MOFs (IRMOF-11 and MOF-14), and a MOF with open metal sites (Zn-MOF-74) for pressures up to 80 bar at 298 K. At low pressures up to 10 bar, the two catenated MOFs showed larger gravimetric CH_4 uptake than the two large-surface-area MOFs due to the higher CH_4 adsorption enthalpy. At higher pressures, however, the two large-surface-area MOFs showed greater gravimetric CH_4 uptake than the catenated MOFs. Although Zn-MOF-74 exhibited only small gravimetric CH_4 uptake due to its high crystal density, it showed the highest volumetric CH_4 storage capacity of 170 v(STP)/v at 298 K and 35 bar, close to the 180 v(STP)/v DOE target for practical CH_4 storage on vehicles.

Several CH_4 adsorption studies have been reported for covalent organic frameworks (COFs),[70,71] which are porous crystalline materials related to MOFs except that they are made entirely of light elements (i.e., no transition metals). Garberoglio[72] simulated CH_4 adsorption in four COFs (COF-102, COF-103, COF-105, and COF-108) for pressures up to 130 bar at 298 K and showed that COF-102 and COF-103 exhibit considerably higher excess volumetric CH_4 uptake than COF-105 and COF-108 because of their higher crystal densities (and thus higher densities of adsorption sites). The results also suggested that COF-102 could meet or exceed the DOE target of 180 v(STP)/v at 35 bar and 298 K. Lan et al.[73] also recently reported CH_4 isotherms in the same COF materials for pressures up to 100 bar at 243 and 298 K. Their excess volumetric CH_4 isotherms in the four COFs agreed qualitatively with those from Garberoglio.[72] They also presented gravimetric isotherms and showed that COF-105 and COF-108 exhibit considerably higher total gravimetric uptakes than COF-102 and COF-103, especially at high pressures. This is exactly contrary to the trends observed in the volumetric uptake. The larger pore volumes and smaller densities of COF-105 and COF-108 gave higher gravimetric uptake but lower volumetric uptake. On the other hand, all four COFs showed similar excess gravimetric uptake of CH_4 at pressures lower than 60 bar. Mendoza-Cortes et al.[74] computationally studied CH_4 adsorption in a variety of COFs, including five 2-D COFs (COF-1, COF-5, COF-6, COF-8, and COF-10) and four 3-D COFs (COF-102, COF-103, COF-105, and COF-108). Among the materials studied, COF-102 and

dx.doi.org/10.1021/cr200217c |Chem. Rev. 2012, 112, 703–723

COF-103 showed the best performances in terms of both total volumetric uptake (255 and 260 v(STP)/v at 100 bar) and the deliverable uptake (229 and 234 v(STP)/v at 100 bar), defined here as the difference in the amount adsorbed at 100 bar versus the amount adsorbed at 5 bar. Considering the structures of COF-102 and COF-103, they argued that a pore diameter of ~12 Å, a large pore volume (>5 cm^3/g), and a high surface area (>5000 m^2/g) can lead to large volumetric CH_4 uptake.

Many of the computational studies summarized above suggest that an optimal adsorbent for CH_4 storage should have a large surface area, a high free volume, a low framework density, the proper pore size, and strong CH_4−adsorbent interactions. Also, many studies have shown that increasing the number of carbon atoms in the organic linkers is a good strategy for improving Q_{st} and increasing CH_4 uptake.

3.1.2. H_2 Storage. There have been several computational studies aimed at developing design criteria for optimal hydrogen storage adsorbents. Frost et al.[75] predicted absolute H_2 isotherms in a series of 10 IRMOFs for pressures up to 120 bar at 77 K. From these simulations, the authors found three adsorption regimes: at low pressures (loadings), H_2 uptake correlates with Q_{st}; at intermediate pressures, H_2 uptake correlates with the surface area; and at high pressures, H_2 uptake correlates with the free volume. In a separate study, Frost and Snurr[76] revisited these correlations for absolute and excess H_2 adsorption at room temperature. They found that absolute H_2 adsorption at 298 K mainly correlates with the free volume throughout the entire pressure range. In addition, they found that, at 298 K and low pressure, excess H_2 adsorption correlates well with Q_{st}, but at high pressure, excess adsorption correlates better with the surface area than with the free volume. In addition, they artificially increased H_2-MOF Lennard-Jones attraction to learn how much Q_{st} must be increased to meet the H_2 storage targets. They found a correlation between Q_{st} and the H_2 density in the pore void volume. On the basis of this correlation, they prepared a graph showing the required Q_{st} as a function of the free volume to meet target gravimetric and volumetric storage amounts at room temperature and 120 bar (Figure 3). The graph suggested that, if new materials with free volumes between 1.6 and 2.4 cm^3/g could achieve isosteric heats of adsorption between 10 and 15 kJ/mol, they could attain H_2 uptakes of 6% at 298 K. The graph provides useful design requirements for obtaining target H_2 loadings within MOFs and other similar microporous materials.

Catenation, where two separate frameworks self-assemble within each other, has been suggested as a means to improve H_2 storage in MOFs. In catenated MOFs, the pore sizes are smaller, leading to stronger H_2/framework interactions, and the number of corner sites, which exhibit stronger binding, is doubled. Therefore, this strategy could increase H_2/framework interactions and thus H_2 adsorption.[5] Jung et al.[6] performed GCMC simulations of H_2 adsorption at 77 K for pressures up to 1 bar in catenated and noncatenated IRMOFs to see the effect of catenation. Their simulation results showed that the small pores generated by catenation can confine the H_2 molecules more densely, so that the capacity of the catenated IRMOFs is higher than that of the noncatenated IRMOFs. Ryan et al.[8] extended this study to higher pressures (up to 120 bar) and ambient temperature. Their GCMC simulations demonstrated that catenation can be beneficial for improving H_2 storage in MOFs at cryogenic temperatures and low pressures but not necessarily at room temperature, as shown in Figure 4. For H_2 storage applications at ambient temperature, their results showed that, for the three

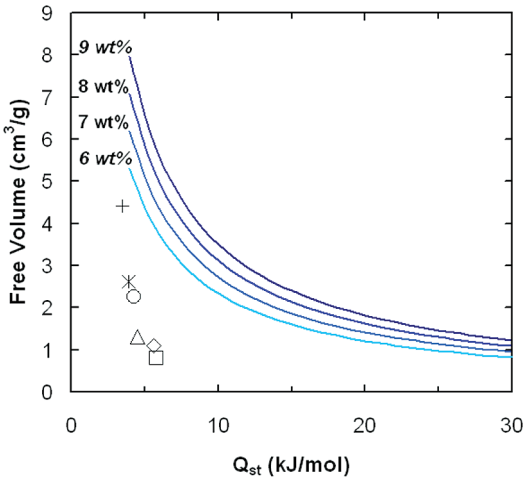

Figure 3. Requirements for target gravimetric H_2 uptake at 120 bar and 298 K. Results for existing materials are marked with symbols: Δ, IRMOF-1; ◊, IRMOF-9; *, IRMOF-10; ○, IRMOF-14; +, IRMOF-16; □, CuBTC. Reprinted with permission from ref 76. Copyright 2007 American Chemical Society.

IRMOFs studied, catenation did not improve adsorption and, in fact, decreased gravimetric uptake significantly. Thus, the authors stated that other strategies for increasing Q_{st} should be pursued to meet H_2 storage targets.

Han et al.[24] calculated H_2 isotherms in 10 different zeolitic imidazolate frameworks (ZIFs), a subclass of MOFs having Zn(II) or Co(II) nodes with imidazolate-type linkers,[77−80] for pressures up to 100 bar at both 77 and 300 K to investigate the effects of functional groups (−C_6H_3Cl, −$C_6H_3CH_3$, −$C_6H_3NO_2$, and −C_6H_4) on H_2 storage. They showed that inclusion of the functional group in the imidazolate linker was helpful for improving the H_2 uptake at 77 K and low pressures because it increased the H_2 binding energy. However, it decreased the H_2 uptake at high pressures due to the decrease in the surface area (or pore volume). They argued that, to obtain high H_2 uptake in ZIFs at both high and low pressures, one should consider ZIFs with not only high surface area but also small pore apertures similar to the kinetic diameter of H_2.

Several recent studies have attempted to use simulation to determine the optimal heat of adsorption in MOFs, i.e., the adsorption enthalpy that maximizes H_2 storage. Frost and Snurr[76] showed that the DOE targets could be achieved even at room temperature if Q_{st} could be significantly increased for MOFs with large free volumes. Thus, a major issue for H_2 storage in MOFs is finding strategies for increasing the heat of adsorption without significant losses in free volume.[81] However, it should be noted that too large an increase in Q_{st} would also increase the H_2 uptake at low pressures and thus decrease the deliverable capacity, which is important in practical applications. Currently, the DOE target storage pressure is 100 bar, and the discharge pressure is ~2 bar. Thus Q_{st} must be large enough to promote significant adsorption at 100 bar but low enough so that H_2 can be released for use at 2 bar. From this, it can be reasoned that there must be an optimal Q_{st} value for attaining the maximum deliverable capacity.

Bhatia and Myers[82] estimated the optimal enthalpy of adsorption for maximizing the deliverable capacity, using a Langmuir adsorption model and considering the storage and delivery pressures of a full adsorption and desorption cycle. They suggested that the optimal Q_{st} for H_2 storage and delivery between 30 and 1.5 bar at

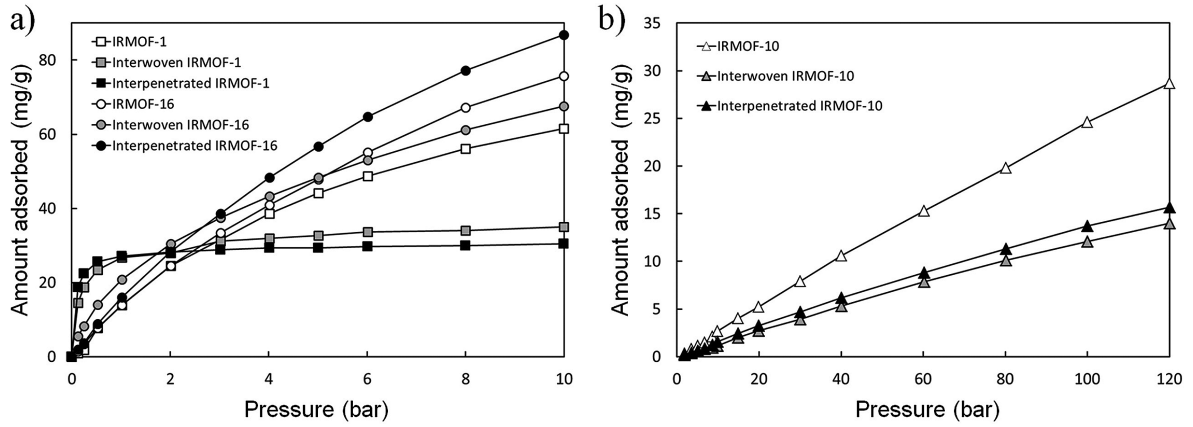

Figure 4. Effect of catenation (interwoven, i.e., minimum distance between frameworks, or interpenetrated, i.e., maximum distance between frameworks) on absolute gravimetric hydrogen adsorption at (a) 77 K and (b) 298 K. Reprinted with permission from Ryan et al.[8] Copyright The Royal Society of Chemistry 2008.

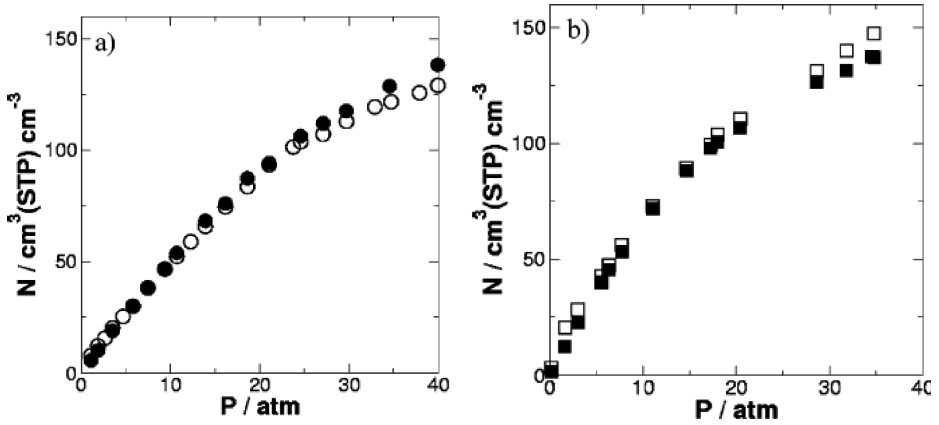

Figure 5. Experimental and simulated methane adsorption isotherms at 298 K: (a) IRMOF-1 and (b) IRMOF-6. Open symbols, experimental results; closed symbols, simulation results. Reprinted with permission from ref 65. Copyright 2004 American Chemical Society.

298 K is 15.1 kJ/mol. They also showed that the corresponding optimal Q_{st} for CH_4 storage and delivery is 18.8 kJ/mol. Later, based on an enthalpy−entropy correlation developed from H_2 adsorption on several cation-exchanged zeolites, Garrone et al.[83] suggested that a considerably higher value of the Q_{st} (22−25 kJ/mol) would be required for optimum H_2 storage and delivery between 30 and 1.5 bar at 298 K.

Recently, Bae and Snurr[84] investigated H_2 storage and delivery in eight representative MOFs for pressures up to 120 bar at 77 and 298 K. They systematically increased the Lennard-Jones ε parameters for H_2/MOF interactions to model the increase in Q_{st} in a general way. Their results demonstrated that the optimal Q_{st} for maximum H_2 storage at 120 bar and delivery at 1.5 bar is ~20 kJ/mol at 298 K. Their results also suggested that a large surface area is more important than a large free volume for obtaining the maximum deliverable capacity of H_2 under these conditions. Thus, they suggested that researchers should concentrate on increasing Q_{st} for MOFs with large surface areas to achieve the H_2 storage targets in terms of the deliverable capacity.

Getman et al.[19] pointed out that, realistically, attempts to increase Q_{st} will generate sites of favorable energy (e.g., cation sites) among regions of unfunctionalized linkers, metal corners, and empty space. They calculated the optimal Q_{st} at those sites, leaving the H_2 interactions in other sites unperturbed, and found that a Q_{st} of 28 kJ/mol is needed to optimize the H_2 deliverable capacity.

3.2. Comparison of Simulated Adsorption Isotherms with Experiment for MOFs and COFs without Strongly Binding Sites

3.2.1. CH_4 Storage. Methane isotherms have been simulated in MOFs and COFs by many groups using GCMC[52,65,68,69,73,74,85,86] and compared with experimental isotherms.[74,87−92] Table S3 in Supporting Information summarizes the force field models used in these GCMC simulations and the level of agreement with experiment. In general, Lennard-Jones potentials with DREIDING or UFF parameters for framework atoms and TraPPE parameters for CH_4 result in good models for understanding CH_4 adsorption in MOFs and COFs.

Düren et al.[65] simulated CH_4 isotherms in IRMOF-1 and -6 at 298 K using a LJ model, and for both materials the simulated isotherms matched well with experimental data from Eddaoudi et al.[87] for pressures up to 40 bar, as shown in Figure 5. Similar results were obtained using DREIDING and UFF force fields, suggesting that these results are not very sensitive to the choice of the framework parameter set. Garberoglio[72] calculated CH_4 isotherms in a series of COFs for pressure up to 130 bar at

dx.doi.org/10.1021/cr200217c |Chem. Rev. 2012, 112, 703–723

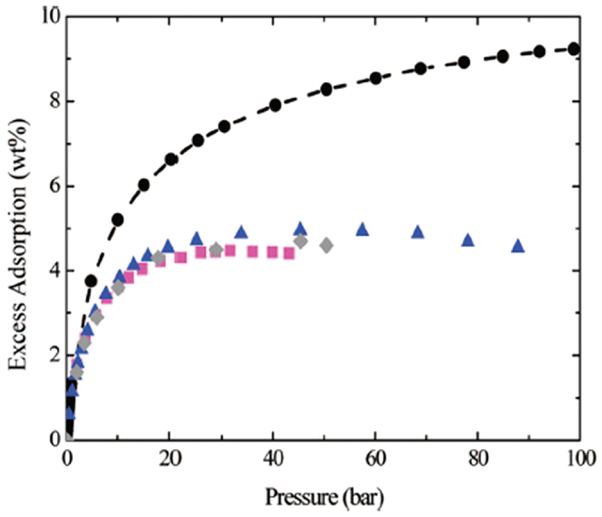

Figure 6. Simulations can show significant deviations from experimental isotherms at high pressure, even if they agree well at low pressure. An example of this is shown for H_2 isotherms in IRMOF-1 at 77 K. Circles, simulations by Yang and Zhong;[102] triangles, diamonds, and squares are experimental data from Wong-Foy et al.,[103] Panella et al.,[104] and Dailly et al.,[105] respectively. Reprinted with permission from ref 25. Copyright 2009 American Chemical Society.

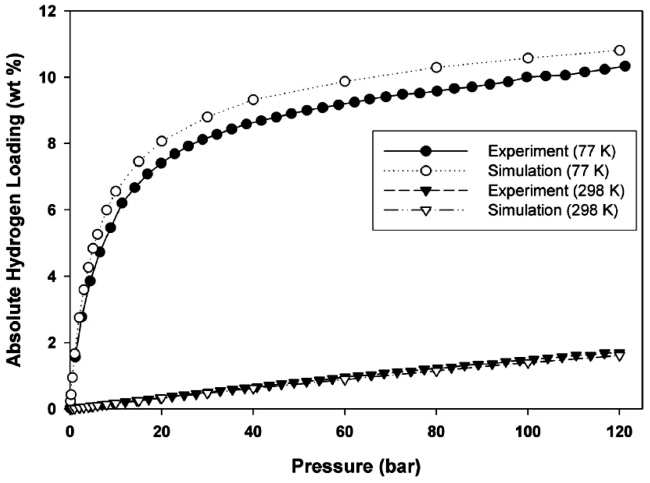

Figure 7. Simulated isotherms for IRMOF-1 compared with experimental isotherms from Kaye et al.[106] Reprinted with permission from Ryan et al.[8] Copyright 2008 Royal Society of Chemistry.

298 K. Unlike the results above for IRMOFs, his simulation results for COFs showed that the CH_4 uptake depends quite significantly on the framework parameters used in the simulation (UFF or DREIDING), which differ by ~20%. Since the UFF model results in a more attractive solid−fluid interaction than DREIDING in these materials, UFF produced systematically higher CH_4 uptake.

There have been several cases where the simulated CH_4 isotherms overestimated the experimental isotherms. These overestimations could come from imperfections in the MOF crystal, such as partial pore blockages or solvent molecules remaining inside the pores. Garberoglio et al.[52] simulated the CH_4 isotherm in a manganese formate MOF for pressures up to 1 bar at 195 K, but the simulation data greatly overestimated the experimental data,[93] which showed very minor adsorption. The authors initially tried to explain these discrepancies in terms of slow diffusion of CH_4 into the MOF. However, they calculated a high diffusivity for CH_4 at low loading, which contradicted their hypothesis. Because their simulations, like essentially all simulations in MOFs, were based on a perfect crystal, it is possible that the discrepancy came from constricted pores due to imperfections in the MOF crystal or solvent molecules remaining inside the pores.[94]

Sometimes authors alter adsorbate or adsorbent force field parameters to achieve a better match with experiment. Wang[68] obtained force field parameters for CH_4 adsorption in $Cu(SiF_6)(bpy)_2$ by fitting some of the OPLS-AA (optimized potentials for liquid simulations-all atom) force field parameters to give a better match with the experimental isotherms.[89] These new parameters have been successfully transferred to predict CH_4 isotherm in $Cu(GeF_6)(bpy)_2$, which matched well with the experimental isotherm.[90]

High level ab initio calculations have also been used to develop force fields that accurately predict the nonbonded interactions between CH_4 and MOF atoms. Lan et al.[73] carried out MP2 calculations to develop force fields for CH_4 adsorption in a series of COFs and calculated CH_4 isotherms at 243 and 298 K. Their simulated isotherm for COF-102 matched reasonably well with the experimental data from Furukawa and Yaghi[92] for pressures up to 100 bar at 298 K but slightly overpredicted the experimental isotherm at high pressures. This overestimation was attributed to imperfections in the sample. Mendoza-Cortes et al.[74] also predicted CH_4 isotherms in a series of COFs based on force fields developed to fit accurate MP2 calculations. Their calculated CH_4 isotherms for COF-5 and COF-8 agreed well with their experimental data for pressures up to 80 bar at 298 K.

3.2.2. H_2 Storage. Although there have been many computational studies of H_2 adsorption in MOFs, only a small portion have been compared with experimental data.[6,8,52,69,76,95−101] In a recent review, Keskin et al.[25] mentioned two important issues that should be considered when comparing simulations with experimental data. The first issue is the pressure range for the comparison. They pointed out that one should not assume that good agreement over a narrow pressure range (e.g., 0−1 bar) will continue to high pressure. Their data show that simulations can deviate significantly from experiments at high pressures, even if they agree well with experiments at low pressures. For an example, see Figure 6. The second issue is the accuracy of the experimental data, because evacuated MOFs may have some imperfections or unremoved solvent. They point out that, even for the same material, there may be considerable deviations among the experimental H_2 uptake from different groups and recommended not developing interatomic potentials based on experimental data from just one material sample.

Table S4 reports the agreement between simulated and experimental hydrogen isotherms from many examples in the literature for a variety of MOFs. The table also reports the different choices made by authors for the H_2 model (spherical LJ, two-site LJ, quadrupole model combined with LJ, etc.) and the MOF LJ parameters (UFF, DREIDING, etc.), as well as whether quantum diffraction effects were taken into account.

Most researchers treat H_2 as a single Lennard-Jones sphere. These models often show better agreement with experimental isotherms than models that explicitly include quadrupole effects, and in some cases, the simulated H_2 isotherms show excellent agreement with experimental data up to high pressures.[8,69,100] For example, Ryan et al.[8] calculated H_2 isotherms in IRMOF-1

for pressures up to 120 bar at 77 and 298 K and obtained excellent agreement with experimental data from Kaye et al.[106] throughout the entire pressure range, as shown in Figure 7.

Garberoglio et al.[52] investigated the effect of including charge−quadrupole interactions between the framework and H_2 as well as quadrupole−quadrupole interactions between H_2 molecules explicitly by using the Darkrim−Levesque (DL) model for H_2.[35] They compared H_2 isotherms calculated in this manner with those calculated using the Buch potential,[107] which treats H_2 as a sphere with a single Lennard-Jones site at the center of mass (no charges), in IRMOF-1 at 77 and 298 K. At 77 K, the simulations from the Buch potential were in reasonably good agreement with the experimental data from Rowsell et al.[108] for pressures up to 1 bar, but the simulations from the DL potential greatly overestimated the experiments. They attributed this overestimation to artificially strong quadrupole−quadrupole interactions between H_2 molecules. However, at 298 K, simulations from both potential models matched reasonably with the experimental results from Rowsell[109] and Panella et al.[104] for pressures up to 70 bar. Gaberoglio et al.[52] noted that the room temperature simulations from both the Buch and DL potentials were almost identical to the each other and concluded that charge−quadrupole and quadrupole−quadrupole interactions are essentially negligible at room temperature and pressures up to 50 bar for H_2 adsorption in IRMOF-1.

One reason that the DL potential may overestimate H_2 uptake at cryogenic temperatures is that it additively combines two independent H_2/H_2 interaction models. The Lennard-Jones interactions were parametrized without considering H_2 partial charges. They implicitly incorporated all types of interactions, including quadrupole contributions, into a Lennard-Jones potential that treats H_2 as a sphere.[40] The Coulomb interactions were independently developed later to model the H_2 quadrupole.[35] Therefore, the DL potential, which is the sum of the Lennard-Jones and Coulomb interactions, may double-count quadrupole contributions. This exposes a need to develop a better model for H_2 that explicitly includes dispersive, repulsive, and quadrupole interactions in a consistent way. For example, Belof, Stern, and Space parametrized a many-body potential that explicitly includes quadrupole and dispersion effects and could suit this purpose.[110]

Quantum diffraction effects are known to be important for H_2 adsorption on carbon-based adsorbents and other porous materials at cryogenic temperatures due to the small mass of H_2 molecules.[111,112] Garberoglio et al.[52] investigated the influence of these effects on H_2 adsorption in IRMOF-1 and IRMOF-8 at 77 K. They used classical LJ potentials and calculated H_2 isotherms with and without considering quantum diffraction effects. Simulations that included quantum diffraction effects used path integral Monte Carlo (PIMC).[113] The simulations were in reasonably good agreement with the experimental data from Rowsell et al.[108] even when quantum diffraction effects were not taken account. Even better agreement was observed at high loadings when quantum diffraction effects were considered, as this slightly reduced the calculated H_2 uptake. Later, Liu et al.[99] did a similar study for H_2 adsorption in HKUST-1 at 77 K. They utilized the Buch potential for H_2 and Lennard-Jones potentials with UFF parameters for framework atoms. They also simulated H_2 adsorption with and without considering quantum diffraction effects and used the Feynman−Hibbs (FH) effective potential[54] to account for quantum diffraction. Simulations performed without taking quantum diffraction into account considerably overestimated their experimental data at high pressures. The FH potential gave the best agreement with experiments at high pressures ∼50 bar. When quantum diffraction effects were considered, the simulated H_2 uptake at 77 K was ∼15−20% lower than results from classical simulations. This agrees with the results of Garberoglio et al.[52]

Several authors have fit force field parameters to better match experiment.[95,96,98] Jung et al.[96] refitted some of the UFF parameters to match experimental H_2 isotherms in IRMOF-1 and IRMOF-18 for pressures up to 1 bar at 77 K. They then applied these modified UFF parameters to simulate H_2 adsorption in IRMOF-3, -9, -11, and -13 at 77 K.[6,96] Their simulations were in reasonable agreement with the experimental data for IRMOF-3, -11, and -13. For IRMOF-9, however, the simulated isotherm greatly overestimated the experimental isotherm, which was ascribed to the loss of crystallinity of the experimental sample upon evacuation.

Researchers have also begun parametrizing force fields using ab initio methods. Han et al.[101] performed MP2 calculations to develop force fields for H_2 adsorption in a series of MOFs and calculated H_2 isotherms at 77 K. The resulting H_2 isotherm in IRMOF-1 agreed well with the experimental data from Rowsell et al.[108] for pressures up to 1 bar. Using similar ab initio calculations, Han et al.[114] successfully developed force fields for H_2 adsorption in a series of COFs, and their simulated H_2 isotherm in COF-5 matched well with their experimental isotherms at 77 K and pressures up to 90 bar. Recently, Han et al.[24] performed a similar study for a series of 10 ZIFs. Their calculated H_2 isotherms in ZIF-8 were in good agreement with the experimental data from Zhou et al.[115] for pressures up to 50 bar at 77 and 300 K.

3.3. Acetylene Storage

Acetylene is an unstable, highly reactive hydrocarbon, and storage is challenging because sufficiently high concentrations can react to form products such as benzene or vinylacetylene. Moreover, these reactions are exothermic so that vessels of acetylene stored at pressures >2 atm risk exploding. Thus high surface-area sorbents for low-pressure acetylene storage have recently been studied.[116−118] Zhang and Chen have recently demonstrated a 40-fold increase, over pure acetylene, for volumetric storage of acetylene at 1 atm using a metal azolate framework.[117] Other novel materials, such as a new MOF-505 analogue,[118] have also demonstrated remarkable acetylene storage capabilities at atmosphere pressure. The isostructural [M_2(DHTP)] MOFs (DHTP = 2, 5-dihydroxyterephthalate and M = Co, Mn, Mg, or Zn; these MOFs are also denoted M-MOF-74,[119] CPO-27-M,[120] and M/DOBDC[121] in the literature) synthesized by Xiang et al. have open metal sites and a high acetylene storage capacity of 230 v(STP)/v at atmospheric pressure for the Co version.[116] Xiang et al. compared the binding energies of acetylene at Co, Mn, Mg, and Zn metal sites in the same MOF and found that Co had the highest affinity for acetylene with a binding energy of 18.5 kJ mol^{-1} followed by 17.3, 16.9, and 16.5 kJ mol^{-1}, respectively.

Along with these materials synthesis reports are recent papers on the simulation of acetylene storage and diffusion in porous materials such as zeolites and MOFs.[122,123] Simulation results have been reported to be in good agreement with experiment, although so far no LJ interaction parameters have been derived for the sp-hybridized carbon atoms in acetylene. Instead, all simulation work so far has used parameters derived for the double-bonded carbons in 2-butene derived in 1984 by Jorgensen et al. in the OPLS force field.[42] Despite this, Fischer et al.

dx.doi.org/10.1021/cr200217c |Chem. Rev. 2012, 112, 703–723

reported excellent agreement between simulated and experimentally measured acetylene uptake in microporous magnesium formate.[122]

4. ADSORPTION IN MOFS WITH OPEN METAL SITES IN THE NODES

Many recent reports of CH_4, H_2, and acetylene storage have focused on MOFs with coordinatively unsaturated "open" metal sites in the nodes or linkers. Such sites have been shown to increase heats of adsorption because they are strongly cationic and can interact favorably with adsorbate multipoles.[19,124,125] The unsaturated nature of the sites along with the stronger adsorbate/adsorbent interactions often make a quantum chemical treatment necessary to understand the interactions. In this section, we discuss how such methods have been used to understand gas adsorption at open metal sites in MOF nodes.

4.1. H_2 Interactions with Open Metal Sites

H_2 interactions with open metal sites in MOF nodes have been calculated by several groups.[69,98,125−129] For example, Kosa et al.[128] used DFT with the BLYP functional to compute H_2 binding energies at Mg^{2+} and Ni^{2+} sites attached to CH_3OCH_3 and OCH_3^- ligands and found Mg^{2+} sites exhibit very weak binding energies of ∼1 kJ/mol, whereas Ni^{2+} sites bind H_2 much more strongly, with binding energies up to 24 kJ/mol. They attributed the increased bond strength to d electron density in Ni^{2+}, which binds favorably with the H_2 $1\sigma^*$ orbital through a Kubas-type[130] interaction. These interactions, discovered by Gregory Kubas in the 1980s,[130,131] involve H_2 binding to transition metals with available d orbitals. A chemical bond is formed due to forward electron donation from the H_2 1σ orbital to metal d and s orbitals and back-donation from metal d orbitals to the H_2 $1\sigma^*$ orbital (Figure 8), causing significant elongation of the H−H bond. Kubas interactions are in general stronger than physical adsorption energies,[19] and thus MOFs with open metal sites available for Kubas binding have attracted interest for H_2 adsorption. However, due to the stronger nature of the H_2/MOF interaction, they cannot be modeled with a simple Lennard-Jones + Coulomb model and require a quantum chemical analysis. For example, Yang and Zhong[98] used periodic DFT in combination with GCMC to calculate H_2 adsorption energies of up to 13.4 kJ/mol at the open Cu^{2+} sites in MOF-505. Sun et al.[125] and Zhou and Yildirim[126] calculated H_2 binding energies at the antiferromagnetic Mn^{2+} sites in Mn_4Cl-MOF[10] of ∼10 kJ/mol. Sun et al. described the binding as an interaction between the H_2 1σ and Mn d_{z^2} orbitals and attributed the relatively weak chemical binding to the formation and occupancy of a high energy antibonding state in the Mn electronic structure. They showed that the lower atomic number metals Sc, Ti, V, and Cr exhibit stronger H_2/metal bonds (up to 46.5 kJ/mol with V) because electrons do not occupy this state. Zhou and Yildirim attributed the bond entirely to Coulombic interactions and suggested the H_2/metal interaction could be strengthened by replacing Cl with less electronegative Br. These results indicate that H_2 adsorption energies at open metal sites can be tuned by using different metals and connecting ligands.

4.2. Methane Adsorption in M-MOF-74

Researchers have also simulated methane adsorption in MOFs with open metal sites. Wu et al.[132] studied CH_4 adsorption in a series of M-MOF-74 materials (M = Mg, Mn, Co, Ni, and Zn), which have high densities of open metal sites. Their CH_4 adsorption isotherm measurements at 298 K and 35 bar for the five M-MOF-74 materials yielded excess CH_4 storage capacities ranging from 149 to 190 v(STP)/v. Among the five isostructural MOFs studied, Ni-MOF-74 showed the highest absolute CH_4 storage capacity (∼200 v(STP)/v). They calculated binding energies of CH_4 on open metal sites using the local density approximation (LDA) and generalized gradient approximation (GGA) DFT methods, and these qualitatively agreed with experimental heats of adsorption. Generally, LDA overestimates the binding energy, whereas GGA underestimates it. They argued that the origin of the high binding energies is due to the unscreened electrostatic interactions between CH_4 and the open metal sites.

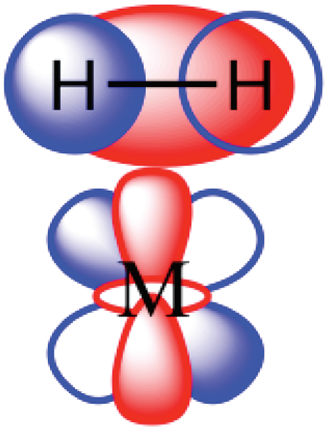

Figure 8. Kubas orbital interactions between a metal ion and the H_2 molecule. Shaded portions indicate regions where the wave function is positive, and open portions indicate regions indicate where it is negative. Red, metal d_{z^2} and H_2 1σ orbitals; blue, metal d_{xz} and H_2 $1\sigma^*$ orbitals; M, metal. Adapted with permission from ref 131. Copyright 1988 American Chemical Society.

4.3. Special Considerations for Calculating Gas Molecule Interactions at Open Metal Sites

Although DFT methods have successfully captured adsorbate/adsorbent interactions at open metal sites, recent work by Grajciar et al.[133] indicates that such methods can be quite inaccurate. Their calculations of H_2O adsorption at the Cu^{2+} sites in HKUST-1 point out two important considerations for modeling gas adsorption at open metal sites: (1) modeling the metal magnetic and spin states correctly and (2) choosing an electron correlation method that accurately captures dispersion and repulsion. They warn researchers to be cautious of results calculated with DFT methods, including DFT+D and related approaches that either add an empirical dispersion term to the DFT results or introduce dispersion perturbatively. Their results indicate that H_2O adsorption energies at HKUST-1 corners are 20 kJ/mol weaker when calculated with DFT than with CCSD(T) due to the inability of DFT to accurately describe dispersion interactions. They additionally show that the DFT+D methods of Grimme[134,135] only partially correct this discrepancy, decreasing the difference to 10 kJ/mol. (However, the same group found DFT+D and SAPT-DFT,[136,137] which is another method that perturbatively includes electrostatic, inductive, and dispersive contributions, performs well for adsorption on graphene surfaces.[138]) We find a similar difference (although opposite in sign) between the H_2 adsorption energies calculated with MP2/6-311+G** and the M06[139] DFT functional using the same basis

dx.doi.org/10.1021/cr200217c |Chem. Rev. 2012, 112, 703–723

set. Using MP2, the binding energy is −6.5 kJ/mol at an equilibrium H_2—Cu^{2+} distance of 2.6 Å, whereas using the M06 DFT method, these values are −12.3 kJ/mol and 2.2 Å, respectively.

As discussed above, MP2 and higher-order methods can require significantly more computer time than DFT, but they can also be significantly more accurate. There is thus motivation to find less computationally demanding yet more accurate methods for describing adsorbate interactions with strongly binding sites. Grajciar et al.[133] proposed the DFT/CCSD(T) approach developed by Bludský et al.[140] as a better way to obtain CCSD(T) level accuracy at reasonable computational efficiency. This method expresses the total DFT error as a sum of error functions calculated from simple one-dimensional pair potentials developed at both the DFT and CCSD(T) levels of theory. It then uses these functions to correct the dispersion in the DFT calculations. In their work, Grajciar et al. found that the DFT/CCSD(T) method exactly reproduces the one-dimensional potential energy surface between H_2O and the HKUST-1 nodes calculated with CCSD(T).

Several researchers have investigated the effect of the magnetic state of open metal sites and have found that, at least in some cases, it can have only a small effect on the interaction energy as long as the number of unpaired electrons is modeled correctly. For example, the $Cu_2(COO)_4$ corners in HKUST-1 are antiferromagnetic in the ground state, and, in agreement with Grajciar et al.,[133] we calculate that the antiferromagnetic singlet is preferred over the ferromagnetic triplet by 15.8 kJ/mol. (Our calculations were performed at the MP2/6-311+G** level of theory.) Note that both of these states have two unpaired electrons; they have opposite spins in the singlet state and parallel spins in the triplet. However, the H_2 binding energies at these sites are nearly identical, −10.2 and −9.5 kJ/mol, respectively. Grajciar et al.[133] obtained similar results for H_2O, calculating a binding energy for the singlet of −52.7 kJ/mol and for the triplet of −52.6 kJ/mol[133] using the highly accurate, multireference CASPT2/ANO-VQZP level of theory. These calculations suggest that adsorbate binding energies are more or less independent of the magnetic state at the Cu^{2+} sites in HKUST-1 corners.[141] Zhou and Yildirim[126] found a similar result for H_2 adsorption at the antiferromagnetic Mn^{2+} sites in the Mn_4Cl-MOF but noted that the number of molecular orbitals containing lone electrons, regardless of the spins of the electrons, considered in the model significantly impacts the H_2 adsorption energy.

5. SIMULATING HYDROGEN ADSORPTION IN MOFS WITH CATION SITES ON THE LINKERS

Another strategy for increasing the enthalpy of adsorption is to introduce open metal sites in the MOF linkers. This strategy is being pursued especially for hydrogen storage. We distinguish between two synthetic approaches for introducing exposed metal sites in MOF linkers, which we refer to as doping[142−144] or functionalization.[13,14] In doped MOFs (Figure 9, left), metal atoms are incorporated into the existing structure through solvothermal reaction, in which metal atoms in solution react with and reduce the framework, forming cationic sites.[142] In the successful experimental examples to date,[142−144] the linkers are chosen for their ability to be chemically reduced. This consideration is not often discussed in simulation studies. In functionalized MOFs (Figure 9, right), the cations are introduced into a

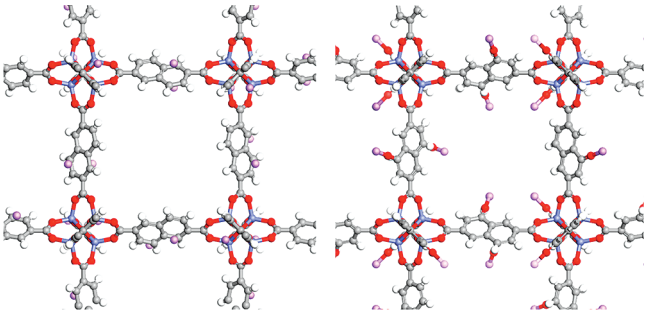

Figure 9. Hypothetical variants of IRMOF-8 with Li cation sites. Left, Li-doped IRMOF-8; right, Li alkoxide functionalized IRMOF-8. Both images are three-dimensional. C, gray; O, red; Li, purple; Zn, blue; H, white.

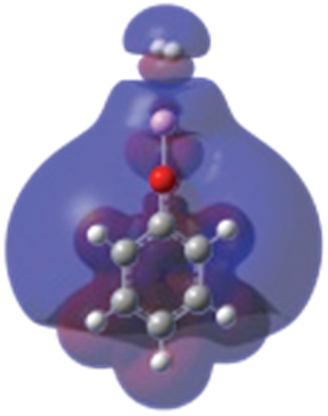

Figure 10. Charge density difference plot for H_2 adsorption at the Li^+ site in Li alkoxide benzene. Blue volumes indicate regions of charge depletion, and red volumes indicate regions of charge accumulation. Atom colors are C, gray; H, white; O, red; Li, purple. Reprinted with permission from ref 19. Copyright 2011 American Chemical Society.

functional group in the linker through an ion-exchange reaction, for example, by reacting a MOF having alcohol groups on the linkers with $Li^+[O(CH_3)_3]^-$, which allows the hydroxyl protons to be replaced by Li^+.[13] Like open metal sites in MOF nodes, metal cations in the MOF linkers exhibit large positive charges,[145] which interact favorably with quadrupolar H_2. As shown in Figure 10 for H_2 adsorption at a Li^+ site, the positive charge on Li^+ interacts with the electron-rich region between the two H nuclei, polarizing H_2 toward Li^+ and resulting in electron density accumulation between H_2 and Li^+.[19] This creates a physical bond.

5.1. Doped MOFs

Simulations of cation doped MOFs build upon similar studies on other carbon-based materials, such as fullerenes and carbon nanotubes.[49,146−155] Although Li is the most common dopant,[49,146,153,155] other alkali,[153] alkaline earth,[149,152] and transition metals[147,148,150,151] have been used as well. Some studies report H_2 adsorption energies of up to 55 kJ/mol on Ti-doped fullerenes.[147,148] However, they show that transition metal dopants prefer to aggregate,[148] decreasing the achievable H_2 adsorption energy. Some groups have reported that, in contrast, alkali and alkaline earth metal cations adhere to the host structure more strongly than they cohere to each other.[146,149] Studies of doped MOFs tend to focus on these metals, specifically Li,[20,50,145,156−164] although transition metals have been examined as dopants as well.[127]

dx.doi.org/10.1021/cr200217c |Chem. Rev. 2012, 112, 703–723

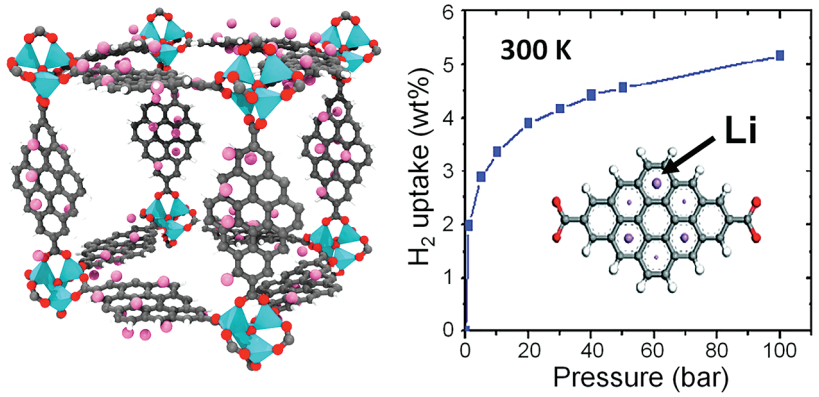

Figure 11. Simulations of H_2 in a Li-doped MOF from Han et al.[20] Left: A model of Li doped MOF-C30, which has six Li dopants on each dibenzocoronene linker; right: hydrogen adsorption isotherm in Li-MOF-C30 at 300 K. Calculations by Han et al. indicate this MOF achieves 5 wt % hydrogen storage at 100 bar and 300 K and 6 wt % hydrogen storage at 100 bar and 243 K (latter result not shown here). Reprinted with permission from ref 20. Copyright 2007 American Chemical Society.

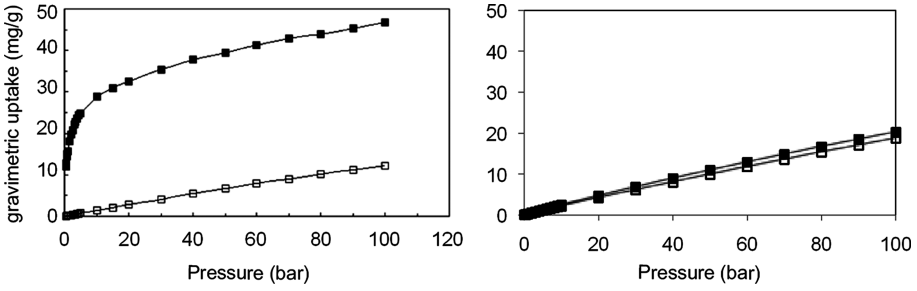

Figure 12. Hydrogen adsorption isotherms in Li alkoxide functionalized (filled squares) and unfunctionalized (open squares) IRMOF-8 calculated by Klontzas et al.[166] at 300 K (left) and in this work at 298 K (right). Isotherms are presented as absolute uptake. Data from Klontzas et al. reprinted with permission from ref 166. Copyright 2008 American Chemical Society.

Han et al.[20] used GCMC calculations to investigate hydrogen uptake in a Li-doped version of MOF-C30, which has dibenzocoronene dicarboxylate ($C_{28}H_{12}(COO^-)_2$) linkers. Their computations suggest that their doped MOF model, which incorporates six Li per linker, can store 6 wt % hydrogen at 100 bar and 243 K and 5 wt % hydrogen at 100 bar and 300 K (Figure 11), thus exceeding the DOE gravimetric target of 5.2 wt % for 2015. They have subsequently filed for a patent for their design.[165] Sun et al.[158] used GCMC to investigate the effect of Li doping into a porous tetrazolide framework and calculated 4.9 wt % hydrogen uptake at 233 K and 100 bar.

Despite the promise suggested by modeling, experimental investigations of cation doping into MOF structures have only been partially successful. Experimental investigations show that cation doping does enhance hydrogen uptake in certain MOFs, but they suggest this is due to cation-induced perturbations of the catenated framework structures and that H_2 molecules do not interact with the cations themselves in the MOFs studied.[142]

5.2. Functionalized MOFs

Compared to doping, linker functionalization has been shown to incorporate metal cations more stably into the MOF structures.[13,14] To date, Li and Mg cations have been experimentally incorporated into MOFs through metal alkoxide functionalization.[13,14] In this strategy, an MOF with alcohol groups on the linker is modified after MOF synthesis to exchange hydroxyl protons for metal cations. Experiments show that Li alkoxide functionalization noticeably enhances hydrogen uptake at cryogenic temperatures and atmospheric pressures, although the observed heats of adsorption are only moderately higher than in unfunctionalized MOFs.[13,14] Several computational studies have examined Li alkoxide functionalization at higher temperatures and pressures,[19,162,166,167] and a recent report from our group details alkaline earth and transition metal alkoxide functionalization and their effects on hydrogen uptake as well.[19] Interestingly, the first computational study of Li alkoxide functionalization by Klontzas et al.[166] was reported prior to any experimental studies.

Computational reports of H_2 adsorption in Li alkoxide functionalized MOFs show conflicting results at ambient temperature, with results from Klontzas et al.[162,166,167] showing significant uptake enhancement at 300 K and results from our group[19] showing negligible uptake enhancement at 243 K (Figure 12). These differences may be due to differences in the model development and are discussed in the next section.

Our calculations indicate that Li alkoxides bind H_2 too weakly (−10 kJ/mol) to overcome the effects of thermal motion near ambient temperatures and are thus not promising functional groups for improving H_2 uptake.[19] Mg, Mn, Ni, and Cu alkoxides bind H_2 much more strongly (−22, −20, −78, and −84 kJ/mol, respectively) and exhibit varying properties. Each Ni or Cu alkoxide binds the first H_2 molecule very strongly but subsequent H_2 molecules much more weakly, with binding energies of −10 kJ/mol or weaker for the second H_2 and beyond. These materials

dx.doi.org/10.1021/cr200217c |*Chem. Rev.* 2012, 112, 703–723

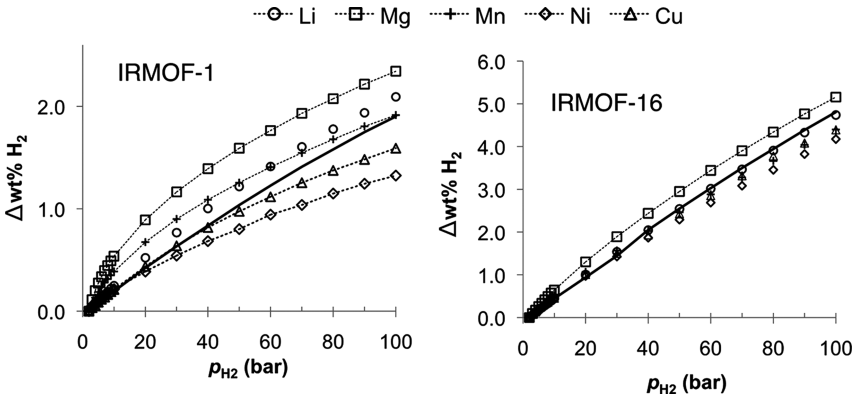

Figure 13. Deliverable hydrogen storage capacities [Δ wt % = wt %(p_{H_2}) − wt %(2 bar)] in metal alkoxide functionalized IRMOF-1 (left) and IRMOF-16 (right) calculated by Getman et al.[19] at 243 K. The solid black lines without symbols represent unfunctionalized MOFs. Reprinted with permission from ref 19. Copyright 2011 American Chemical Society.

thus take up significant amounts of hydrogen at low pressures, but then uptake levels off. They are thus ineffective as automotive H_2 storage materials, because they do not release significant H_2 for use at the release pressure of 2 bar. Mg and Mn bind H_2 much more weakly. Of these, Mg forms a more flexible bond with H_2 and is lighter in weight. Our calculations indicate Mg alkoxide functionalized IRMOF-1, IRMOF-10, IRMOF-16, UiO-68, and UMCM-150 exhibit superior deliverable capacities (Figure 13). In fact, we find that Mg alkoxide functionalized IRMOF-16, which has theoretical surface area and pore volume of over 6000 m^2/g and 4 cm^3/g, respectively, achieves a deliverable capacity of 5.2 wt % at 100 bar and 243 K, meeting the DOE gravimetric target for 2015.

5.3. How Simulation Methods Impact Gas Adsorption Results

Simple Lennard-Jones + Coulomb force fields do not adequately describe the strong interactions between gas molecules and open metal sites as shown for one example in Figure 14. Therefore, GCMC simulations of such systems often require new force fields, and a common method of development is to derive the parameters from quantum mechanics.

There are many challenges to creating such force fields. First, due to limitations in computer resources, quantum calculations must be carried out on small models of the material, and these models must be carefully selected to ensure the electronic structure in the model closely resembles that of the open metal site in the MOF. Second, these pair potential models only consider a single adsorbate interacting with the adsorbent. The energy changes that occur when multiple molecules adsorb are treated in an additive way, and this ignores many-body contributions to the energy. Third, as with all adsorption calculations, the models and methods used in the quantum chemical calculations must accurately capture the chemistry of the interaction. We discuss these challenges in this section.

5.3.1. Effect of Interaction Model on Calculated H_2 Adsorption Uptake. Computational details may have a noticeable effect on the overall results. For example, in Li-doped systems, the Li^+ site model used in the quantum chemical calculations can significantly impact the calculated H_2 uptake. To illustrate this, we calculated H_2 adsorption isotherms on a Li-doped version of IRMOF-8, modeled with one Li cation per linker. We used three different force fields to describe the H_2 interaction with Li^+. Two of these were developed in this work using two different Li^+ site models, and the third was taken from the work of Deng et al.[49] We used these

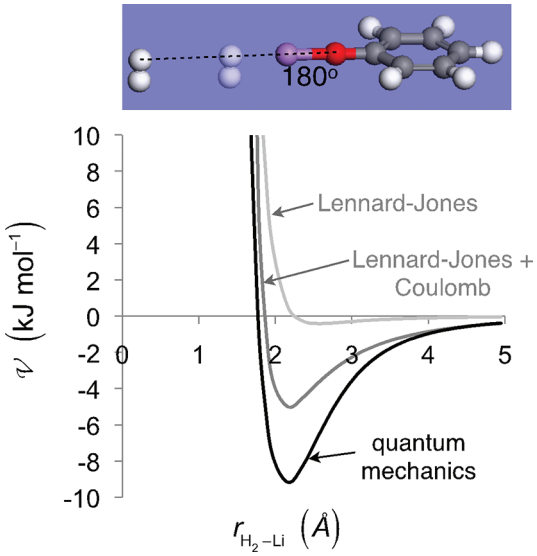

Figure 14. Potential energies ($\mathcal{V}$) for a H_2 molecule approaching Li alkoxide benzene at a particular angle. Force field energies computed with Lennard-Jones potentials use DREIDING parameters[44] for Li alkoxide benzene atoms and empirically derived parameters[40] for H_2. Cross-term parameters were obtained using the Lorentz−Berthelot mixing rules. Partial charges on Li alkoxide benzene atoms were calculated using the ChelpG method,[36] and partial charges on H_2 were taken from the Darkrim−Levesque model.[35] Quantum mechanical energies (black) were computed at the MP2/6-311+G** level of theory, using counterpoise corrections[64] to correct for basis set superposition.

force fields to describe H_2 interactions with Li^+, and we used conventional force fields to describe H_2 interactions with all other framework atoms. We have previously described this procedure in depth,[19] and more details can be found in the Supporting Information. The force fields developed in this work were parametrized by fitting a pair potential to the differences in electronic energies for H_2 adsorbed in a variety of configurations surrounding the Li^+ site,

$$\Delta E(r) = E^{\text{elec}}_{\text{Li}^+ - \text{H}_2}(r) - E^{\text{elec}}_{\text{Li}^+} - E^{\text{elec}}_{\text{H}_2} \quad (5)$$

where Li^+ broadly describes the model containing the open Li^+ site. Values of ΔE for the first force field parametrization were calculated for interactions between H_2 and a bare Li^+ cation at the MP2/6-311+G** level of theory and fit to a Morse potential. Note that this

dx.doi.org/10.1021/cr200217c |Chem. Rev. 2012, 112, 703–723

H_2/Li^+ system has a net charge of +1, which was taken into account in the quantum calculations. However, all species were considered to be neutral in the pair potentials and GCMC calculations, i.e., the charge−quadrupole interactions were incorporated into the Morse potential instead of being added as separate terms.

For the second force field parametrization, we used a similar procedure, this time using potential energies calculated between H_2 and a $Li^+(C_{10}H_8)^-$ model (Figure 15) at the same level of theory. Note that Li in this system adopts a partial positive charge and $C_{10}H_8$ adopts the opposite negative charge, but the system as a whole is charge-neutral. Here we only developed parameters to describe the H_2/Li^+ interaction, and H_2 interactions with all other atoms were simulated using conventional force field models (see the Supporting Information). H_2 binding energies, defined as the changes in electronic energies at the optimal adsorption geometry, to the bare Li^+ cation and $Li^+(C_{10}H_8)^-$ models are provided in Table 1. Note that H_2 binds much more favorably to the bare Li^+, which exhibits a binding energy of −22 kJ/mol compared to −12 kJ/mol for $Li^+(C_{10}H_8)^-$. For the third H_2/Li^+ force field, we used parameters from Deng et al.,[49] which were developed in 2004 and are still used in GCMC calculations of H_2 adsorption in Li-doped materials today.[20,50] H_2 adsorption results are shown in Figure 16, and Q_{st} values at low loading (<1 H_2 per Li^+ site) are provided in Table 2. The simulations performed using different force fields yield dramatically different results. Absolute loadings at 100 bar in Li-doped IRMOF-8 are 2.9, 2.5, and 3.4 wt % using the Li^+, $Li^+(C_{10}H_8)^-$, and Deng potentials (to be compared with 1.8 wt % in nondoped, unfunctionalized IRMOF-8.) These qualitatively follow the order of Q_{st}, which are 21.6, 12.5, and 25.9 kJ/mol, respectively. Q_{st} calculated using the Li^+ and $Li^+(C_{10}H_8)^-$ force fields closely resemble the H_2 binding energies to those systems (provided in Table 1), and the Q_{st} calculated using the Deng potential[49] is similar to the binding energy to a bare Li^+.

To our knowledge, there is only one experimental result for Li doping available for comparison. Li et al.[50] measured H_2 uptake in a Li-doped polymer and observed a maximum Q_{st} of 8.2 kJ/mol. Q_{st} depends on a variety of factors, such as the temperature and pressure at which measurements were taken, structural properties (e.g., presence of imperfections or leftover solvent molecules in the MOF), gas loading, and the local environment surrounding the Li^+ site, and thus we cannot directly compare this experimental value with the ones calculated in this work. A qualitative assessment indicates that Q_{st} for the H_2/Li-doped system is quite modest and similar to that obtained using the force field developed with the $Li^+(C_{10}H_8)^-$ model. In constrast, the Q_{st} obtained from simulations using the Li^+ and Deng force fields are significantly larger and concomitantly result in much larger H_2 uptakes. The $Li^+(C_{10}H_8)^-$ model is certainly more realistic than the Li^+ model, so it is unsurprising that the resulting force field yields a Q_{st} more in line with experimental observation.

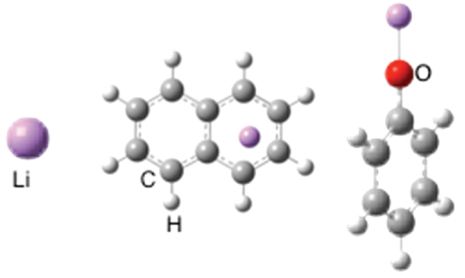

Figure 15. Models used to create H_2/Li^+ force fields. A bare Li^+ cation (left), $Li^+(C_{10}H_8)^-$ (middle), and Li alkoxide benzene (right).

Table 1. H_2 Binding Energies to Various Li Cation Site Systems Calculated Using MP2/6-311+G**

system	ΔE (kJ/mol)
Li^+	−22
$Li^+(C_{10}H_8)^-$	−12
Li alkoxide benzene	−10

Table 2. Isosteric Heats of Adsorption (Q_{st}) for H_2 in Li-Doped and Li Alkoxide Functionalized IRMOF-8 Calculated with GCMC at 77 K Using Different Force Fields; All Values Are for Points on the Isotherm with <1 H_2 per Li^+ Site

IRMOF-8 variant	force field	Q_{st} (kJ/mol)
Li-doped	Li^+	21.6 ± 0.02
	$Li^+(C_{10}H_8)^-$	12.5 ± 0.07
	Deng et al.[49]	25.9 ± 0.06
Li alkoxide functionalized	Li alkoxide benzene, MP2/6-311+G**[19]	9.9 ± 0.14
	Klontzas et al.[167]	22.0 ± 0.03

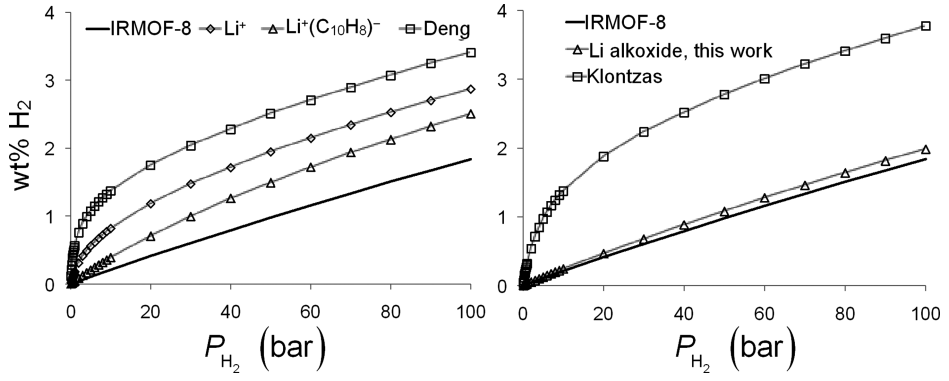

Figure 16. H_2 absolute adsorption isotherms for Li-doped (left) and Li alkoxide functionalized (right) IRMOF-8 at 298 K. Isotherms were calculated using a variety of potentials and parameters to describe H_2 interactions with the Li^+ site. See the main text and Supporting Information for details. The solid black lines without symbols are for nondoped, unfunctionalized IRMOF-8.

dx.doi.org/10.1021/cr200217c |Chem. Rev. 2012, 112, 703–723

These results highlight how H_2 adsorption results are directly related to the force fields. To illustrate this further, we performed a second set of calculations, this time comparing H_2 adsorption isotherms for Li alkoxide functionalized IRMOF-8 using two sets of parameters for alkoxide O and Li. The first set we took directly from our previous work,[19] which fit ΔE between H_2 and Li alkoxide benzene models calculated at the MP2/6-311+G** level of theory to a Morse + Coulomb potential. The second set are Lennard-Jones parameters taken from Klontzas et al.[167] All parameters, as well as a more detailed explanation of the parametrization procedure, are provided in the Supporting Information. H_2 adsorption isotherms calculated at 298 K using these different parameter sets are shown in Figure 16, and Q_{st} calculated at low loading are shown in Table 2. Differences in the calculated uptakes are even greater for Li alkoxide functionalized IRMOF-8 than in Li-doped IRMOF-8, with potentials from our work projecting an uptake of 2.0 wt % and potentials from Klontzas projecting an uptake of 3.8 wt % at 100 bar. These again can be related to the Q_{st} values, which are 9.9 and 22.0 kJ/mol, respectively. There are at least two experimental results that we can compare with these values. Mulfort et al.[13] measured H_2 uptake in a MOF with dipyridine glycol linkers, with 10% of the hydroxyl H^+ substituted for Li^+, and observed a maximum Q_{st} of 6.6 kJ/mol. Himsl et al.[14] performed a similar study of Li alkoxide functionalized MIL-53(Al) and measured a maximum Q_{st} of 11.6 kJ/mol. Again, these values are quite modest.

5.3.2. Limitations of Pair Potential Models. In pair potential models, the potential energy $\mathcal{V}$ of an interaction between an adsorbate and an adsorbent is modeled by summing the interactions between the atoms in the adsorbate and the atoms in the adsorbent, as if each interaction were completely isolated. Both dispersive and Coulombic interactions are treated in this manner. However, these models fail to capture many-body interaction terms, which can be significant even in nonbonding interactions.[62,168,169] For example, as shown by von Lilienfeld and Tkatchenko,[62] many-body contributions can contribute up to 10% of dispersive energies. In addition, current force fields are completely ineffective at capturing dynamic behavior in the electronic structure, such as polarization and charge transfer. Potential models that include these terms have been developed,[62,110] but they are not in widespread use.

The multi-Langmuir approach used by Sauer and co-workers[170−173] is one way to completely avoid the need for a force field. In the multi-Langmuir approach, geometry optimizations of the adsorbate are performed at different binding sites at the MOF surface using quantum mechanics. Typically, small MOF fragments are used because of computational constraints. However, Sauer and co-workers[170−173] have developed a method where the full MOF is included: they use density functional theory to compute long-range interactions and a higher level of theory such as MP2 to compute short-range interactions. In the multi-Langmuir approach, the number of molecules at the different sites are added together, neglecting interactions among molecules, as in the standard multisite Langmuir model,[174] and this is used to compute the uptake. (Sometimes researchers simply estimate the maximum loading by calculating the number of sites and then assuming one molecule per site.[145,146,148,149,153,155,175]) The multisite Langmuir equation[170] requires the adsorption equilibrium constant K^{eq} for each site. This can be obtained from the partition functions, Z, of the adsorbed molecule and the molecule in the gas phase[170−173]

$$K^{eq} = \frac{Z_{adsorbate}}{Z_{gas}} e^{-D_0/RT} \quad (6)$$

where $D_0 = \Delta E^{elec} + \Delta E^{ZP}$ (i.e., D_0 is the potential energy $\mathcal{V}$ at the local minimum on the potential energy surface). The ratio of partition functions represents the changes in translational, rotational, and vibrational entropies due to adsorption. Using this model, the translational and rotational entropies of the adsorbate are considered to be zero, and the adsorbate vibrational entropy is calculated using the calculated vibrational modes of the adsorbate. (Changes in adsorbent vibrational modes are typically considered to be negligible.) Note that this treatment does not include configurational contributions to the entropy, which can be significant both at high temperature and when the number of adsorbate molecules is large.

5.4. Challenges in Force Field Development

Given that simulations can be used to guide experiments (and even influence the decisions of funding agencies), force field development is of utmost importance. One of the challenges in developing highly accurate force fields from quantum chemical calculations is that the quantum chemical calculations must be performed with extreme care, using the most realistic models and the most accurate level of theory possible, which can be very time-consuming. As discussed above, MP2 electron correlation is feasible for many systems of interest (but it also has its own limitations). For example, we performed hundreds of MP2 single-point calculations of the H_2/Li alkoxide benzene system (in series) to develop the force field described in ref 19, and the calculations were easily performed on a single Intel computing node with dual quad core processors.

The model system also affects computational expense. For example, it takes significantly less time to compute the energy of a H_2/Li^+ system at the MP2/6-311+G** level of theory than it does to calculate the energy of a $H_2/Li^+(C_{10}H_8)^-$ system at the same level of theory. However, as discussed above, the bare Li^+ cation ultimately yields an unrealistically large Q_{st} and thus H_2 uptake, making a more realistic model necessary.

Balancing accuracy and expense is one of the biggest challenges in performing quantum chemical calculations. In general, the most realistic models and the most accurate level of theory possible should be used to ensure the most accurate results. To add credibility to any results obtained using force fields developed from quantum calculations, the computational procedures should be reported in detail. We recommend reporting the following details *at minimum*: the model system, the electron correlation method and basis set, other relevant details about the quantum chemical calculations (e.g., whether or not counterpoise calculations were used), the number of single points used to perform the parametrization (e.g., whether the parameters were developed by allowing the gas molecule to follow a single path to the adsorption site or whether more of the potential energy surface of interaction was taken into account, as in ref 19), and some measure of how well the force field replicates the ab initio data. The final force field itself, including the potentials used and the final set of parameters, should also be reported. Additionally, a detailed comparison with either experiment or higher levels of theory should be made if possible, and any expected limitations in the final force field should be thoroughly discussed.

Even the best reported force fields today leave room for improvement. For example, most force fields are parametrized to fit the electronic interactions between a single H_2 and a Li^+ site model, but H_2/H_2 interactions are not considered in the parametrization. In GCMC calculations, the H_2/H_2 interactions are typically calculated using a Lennard-Jones model, which does not take the differences in the H_2 electronic structures near the adsorption site into account. For example, a H_2 molecule adsorbed to a metal site in a Kubas-type

complex is chemically bound. As more H_2 molecules adsorb to the metal site, they interact with the initial H_2 molecule through dispersive, repulsive, and quadrupole interactions, which can be captured with a Lennard-Jones or Lennard-Jones + Coulomb model. However, the H_2 binding energies are collectively affected by other chemical phenomena as well, such as competition for d electrons at the metal site. Subsequent H_2 molecules are also forced to bind in new configurations, which require different orbital interactions between the adsorbate and the metal site, and those configurations may not be as energetically favorable. These effects all weaken the adsorption energies at metal sites, but force fields parametrized without explicitly including the interactions between adsorbed H_2 do not capture them.

Additionally, force fields rarely include polarization, thus treating Coulombic interactions in a static manner. Methods for treating polarization have been proposed,[176,177] but they require an iterative approach, significantly increasing the time needed to complete the GCMC calculations. Such effects can be explicitly calculated, for example, by using periodic electronic structure calculations. However, such calculations are expensive and thus limited to density functional theory methods, which are notoriously inaccurate for describing dispersive interactions. Additionally, DFT and other ab initio-based methods neglect the effect of temperature, most notably the entropic contributions to the free energy. Even the multi-Langmuir approach discussed above neglects configurational entropy, which can be significant in gas adsorption. There are thus clear opportunities to improve the methods used to calculate gas adsorption at strongly adsorbing sites.

In this review, we have focused on modeling MOFs that are generally rigid and do not undergo large structural transitions in response to adsorption. Even these MOFs, however, have small-scale, local softness and flexibility. Several groups have tested how this local flexibility influences gas adsorption by performing simulations that allowed framework atoms to move in response to gas uptake (i.e., flexible-framework simulations). They found that simulations assuming a completely rigid framework agree well with flexible-framework simulations when the framework is fairly stiff (i.e., when allowing the framework to relax in response to gas uptake results in only small structural changes) and the temperature is low.[178,179] For another class of MOFs, such as MIL-53,[180,181] the framework is sufficiently flexible that its geometry can change dramatically under high pressure.[182] Here there are two distinct challenges: predicting the structural conformations under various conditions (e.g., pressure and temperature) and subsequently predicting gas adsorption using either a rigid structure derived from the prior step or a more sophisticated approach such as osmotic framework adsorbed solution theory (OFAST).[183,184] OFAST[185,186] considers a discrete number of structural phases of a flexible MOF in an osmotic thermodynamic ensemble. Predicting the structural phases has been approached using both QM (quantum mechanical) and MM (molecular mechanics) methods,[187] although only the latter can incorporate thermal phenomena, such as the negative thermal expansion in IRMOF-1.[188] Salles et al. specifically parametrized the Cr−O bonded intramolecular term in MIL-53 so that molecular dynamics (MD) simulations reproduced the cell volumes measured via in situ powder X-ray diffraction.[189] Testing new force fields via molecular dynamics simulations can be computationally expensive, and Dubbeldam et al. report an efficient energy-minimization scheme for this purpose, which they tested by reproducing MIL-53 transitions under water loading.[190]

In principle, a hybrid MD-GCMC simulation approach could capture the effects of adsorption during a continuous structural transition of a highly flexible MOF, but to our knowledge there are no reports of this kind in the literature. Developing accurate force fields for flexible MOFs that simultaneously predict structure transitions and correct gas adsorption is a rich area for further research.

6. CALCULATING HEATS OF ADSORPTION

One of the most important properties of gas storage materials is the enthalpy or "heat" of adsorption Q_{st}. This quantity can be easily calculated in GCMC simulations. As reviewed by Vuong and Monson[191] and others,[192−199] there are many related adsorption enthalpies that have been defined in the literature, and some reports do not carefully distinguish which value is reported. A widely used quantity is the isosteric heat of adsorption, Q_{st}, which is defined as the differential amount of heat $\mathcal{Q}$ added to an adsorbent/adsorbate system due to a differential change in the number of moles N of adsorbate at constant temperature T.[193]

$$Q_{st} = \left(\frac{\delta \mathcal{Q}}{\delta N}\right)_T \tag{7}$$

For a gas phase at constant T, pressure P, and chemical potential μ in equilibrium with an adsorbed phase at constant T, volume V, and μ,[191,194]

$$Q_{st} = T\left[\left(\frac{\partial N\underline{S}}{\partial N}\right)_{T,P} - \left(\frac{\partial N\underline{S}}{\partial N}\right)_{T,V}\right] \tag{8}$$

where $\underline{S} = S/N$ and S is the entropy.[200] At equilibrium, the chemical potentials in the two phases are equal,

$$\mu^{\text{gas phase}} = \left(\frac{\partial(N\underline{G})}{\partial N}\right)_{T,P} = \left(\frac{\partial(N\underline{H})}{\partial N}\right)_{T,P} - T\left(\frac{\partial(N\underline{S})}{\partial N}\right)_{T,P} \tag{9}$$

and

$$\mu^{\text{sorbate phase}} = \left(\frac{\partial(N\underline{A})}{\partial N}\right)_{T,V} = \left(\frac{\partial(N\underline{U})}{\partial N}\right)_{T,V} - T\left(\frac{\partial(N\underline{S})}{\partial N}\right)_{T,V} \tag{10}$$

Here H, U, G, and A are the enthalpy, internal energy, Gibbs free energy, and Helmholtz free energy, respectively. Substituting eqs 9 and 10 into eq 8 yields[191]

$$Q_{st} = \bar{H} - \left(\frac{\partial(N\underline{U})}{\partial N}\right)_{T,V} \tag{11}$$

where $\overline{H}$ is the partial molar enthalpy in the gas phase. In terms of molecular properties[58]

$$Q_{st} = \bar{H} - \left(\frac{\partial\langle N\rangle\langle \mathcal{V}\rangle}{\partial\langle N\rangle}\right)_{T,V} \tag{12}$$

where the brackets indicate ensemble average quantities, taken here in the grand canonical ensemble. Equations 11 and 12 are general.[191] However, they are often simplified by making assumptions about the gas and adsorbate phases. To perform such simplification, we write $\overline{H}$ as

$$\overline{H} = \overline{U} + P\overline{V} \tag{13}$$

dx.doi.org/10.1021/cr200217c |Chem. Rev. 2012, 112, 703–723

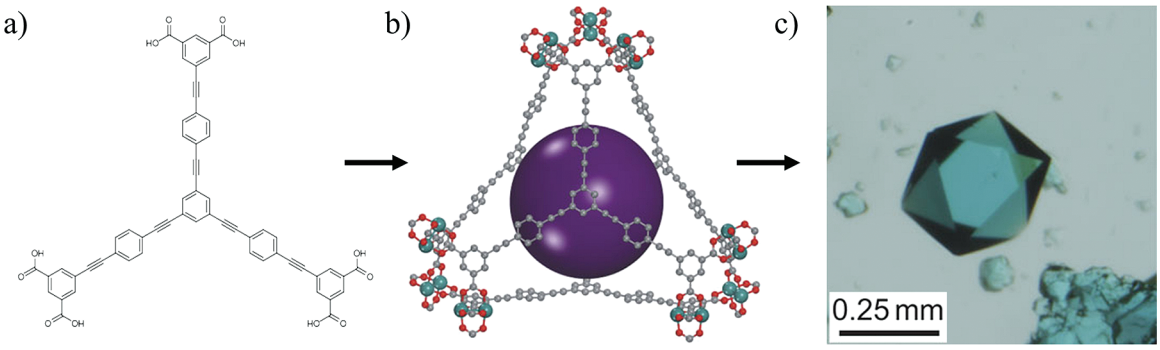

Figure 17. A new organic linker (a) was designed, and the resulting crystal structure (b) was predicted computationally. Subsequent synthesis yielded a material (c) whose structure was in excellent agreement with the computational predictions. Figure adapted from ref 2. Copyright 2010 Nature Publishing Group.

and note that the gas-phase properties can be separated into ideal and residual contributions

$$H = H^{\text{ideal}} + H^{\text{R}} \tag{14}$$

where the superscript R indicates the residual quantity.[195] If we set $\langle \mathscr{V}^{\text{ideal}} \rangle$, the potential energy of the ideal gas, as the thermodynamic reference state, then we can rewrite eq 12 as

$$Q_{\text{st}} = \langle \Delta \mathscr{V} \rangle + P[\bar{V}^{\text{ideal}} + \bar{V}^{\text{R}}] - \left(\frac{\partial \langle N \rangle \langle \Delta \mathscr{V} \rangle}{\partial \langle N \rangle} \right)_{T,V} \tag{15}$$

where $\Delta \mathscr{V}$ is the potential energy deviation from that of the ideal gas.[201] If the gas phase is ideal, then[196]

$$Q_{\text{st}} = RT - \left(\frac{\partial \langle N \rangle \langle \Delta \mathscr{V} \rangle}{\partial \langle N \rangle} \right)_{T,V} \tag{16}$$

which is the familiar form of Q_{st} used in many GCMC simulations. Even if the gas phase is nonideal, eq 16 is still valid as long as the errors in $\langle \mathscr{V} \rangle$ and $\langle N \rangle$ are greater than the nonideality corrections.[202] The isosteric heat can easily be calculated during GCMC simulations and used to assess and screen MOFs as gas storage materials.

7. USING SIMULATIONS TO GUIDE EXPERIMENT

Although a holy grail of computational simulation in this field, yet to be achieved, is to predict an ideal gas storage material entirely from simulations, a number of steps in this direction have already been successfully demonstrated. As described above, Düren et al.[65] proposed a novel MOF for methane storage, IRMOF-993, with a novel linker, and Ma et al.[16] tried to synthesize it. Although IRMOF-993 is perhaps not synthetically accessible, the ideas of Düren et al. about linker design further inspired Ma to synthesize additional materials, including PCN-14, which exhibited record methane storage.

More recently, the MOF NU-100 provides another example of the power of simulation to guide experiment. This MOF was constructed on the computer and evaluated for high surface area and gas uptake *before* it was synthesized.[2] On the basis of the promising results from simulation, the material was synthesized and found to closely match the structure that was simulated a priori. The organic linker of NU-100 (see Figure 17) was chosen to imbue the resulting crystal structure with a high gravimetric surface area (measured Brunauer–Emmett–Teller (BET) surface area = 6 143 m^2/g).[2] The resulting structure had a high storage capacity for H_2 (164 mg/g absolute) at 70 bar and 77 K in excellent agreement with predictions from modeling. The excess hydrogen storage exhibited by this material (99.5 mg/g) is the highest reported to date at 77 K.

Simulations may also be used to screen libraries of existing MOFs. Keskin, Haldoupis, and Sholl have screened hundreds of MOFs recently to identify the most promising materials for kinetic gas separations (a related application to gas storage).[203,204] As computational resources continue to expand exponentially, reports of increasingly larger-scale screening of MOFs are becoming more common.[205] In the near future, one may expect that large-scale screening efforts will allow for the identification of promising *hypothetical* MOFs, as was done for NU-100, but in a systematic fashion.

8. CONCLUSIONS AND OUTLOOK

Molecular simulation is an important tool for understanding gas adsorption in MOFs and other porous materials. Simulations have been used for understanding molecular-level phenomena, predicting uptake, verifying experimental observations, screening MOFs for various applications, and other purposes. One of the most important applications of simulations is guiding material design.

First-generation simulations of gas adsorption in porous materials have used classical potentials with the MOF parameters from rather generic force fields. These models do a reasonably good job of describing gas adsorption in materials with no open metal sites or other functional groups that interact strongly with guest molecules. For example, simulations performed with these force fields have provided numerous insights into methane and hydrogen adsorption in MOFs. They have also suggested useful criteria for designing optimal MOFs for storing these gases.

These force fields are less successful at capturing adsorption phenomena in materials with strongly binding sites, such as open metal sites or large electric fields. New force fields are needed to describe gas interactions in frameworks with such features, and these are typically derived from quantum chemical calculations. The key challenges in developing such force fields are selecting the model systems on which to perform the quantum chemical calculations and selecting the appropriate level of theory. These challenges are complicated by the computational expense often associated with using better models and methods. For example, we have shown here that using a bare Li^+ cation as a model system to explore H_2 interactions with Li cations incorporated in MOF linkers overestimates the H_2 adsorption enthalpy and thus the predicted uptake. A more representative model includes part of the MOF linker. However, a larger system includes more electrons, which increases the computational resources needed to develop the force field.

dx.doi.org/10.1021/cr200217c |*Chem. Rev.* 2012, 112, 703–723

Several reports covered in this review have used quantum chemical methods along with GCMC simulations to screen and assess MOFs for gas storage applications. Some of this work has motivated subsequent experimental design. Despite these successes, further work in force field development is needed. The work reviewed here indicates the need for models that accurately capture (1) chemical interactions at adsorption sites, specifically those that exhibit strong binding energies, and (2) dispersive, repulsive, Coulombic, polarization, and multipole effects simultaneously. The quantum chemical-based force fields do a reasonable job of capturing these phenomena in some systems. However, there is a need for even more advanced force fields.

The simulation methods available today are able to capture many key features associated with gas adsorption in MOFs, including those with strongly binding sites. As discussed in this review, molecular simulations have been highly successful in understanding gas adsorption in porous materials. As advancements in computers, models, and simulation algorithms are made, simulations will become even more powerful in aiding understanding and material design.

ASSOCIATED CONTENT

Supporting Information

Detailed comparisons of theoretical and experimental data and descriptions of force field parametrization procedures can be found in the Supporting Information. This information is available free of charge via the Internet at http://pubs.acs.org/.

AUTHOR INFORMATION

Corresponding Author

*E-mail: snurr@northwestern.edu.

Present Addresses

[†]Department of Chemical and Biomolecular Engineering, Clemson University, Clemson, SC 29634, United States.

BIOGRAPHIES

Rachel B. Getman received her Ph.D. in Chemical Engineering from the University of Notre Dame in 2009 under the direction of Prof. William F. Schneider. She was a Postdoctoral Research Fellow with Prof. Randall Q. Snurr at Northwestern University from 2009 until 2011. In the fall of 2011, she joined the Department of Chemical and Biomolecular Engineering at Clemson University as an Assistant Professor. Her research involves molecular modeling of adsorption and heterogeneous catalysis, with special emphasis on catalyst design.

Youn-Sang Bae received his Ph.D. in Chemical Engineering in 2006 at Yonsei University (Korea), under the supervision of Prof. C.-H. Lee, in the field of adsorptive separation process. Following postdoctoral work with Prof. Snurr, he was promoted to research assistant professor at Northwestern University in 2010. In the spring of 2012, he will join the Department of Chemical and Biomolecular Engineering at Yonsei University as an Assistant Professor. His research involves experimental and computational studies of metal−organic framework materials for energy storage and various separations.

Christopher E. Wilmer received his B.A.Sc. degree in Engineering Science with a specialization in Nanoengineering from the University of Toronto. He is currently a Ph.D. candidate in Chemical Engineering at Northwestern University, where he holds a Ryan Fellowship. His research interests include computational screening and design of porous crystalline materials and scientific illustration and visualization.

Randall Q. Snurr received his Ph.D. in Chemical Engineering in 1994 from the University of California, Berkeley. After postdoctoral research at the University of Leipzig (Germany), he joined the faculty at Northwestern University, where he is currently a Professor of Chemical and Biological Engineering and a Senior Editor for the *Journal of Physical Chemistry*. His research interests include computational modeling and design of new materials for applications in separations, catalysis, gas storage, and sensing.

ACKNOWLEDGMENT

This work was funded by the Department of Energy under grant number DE-FC36-08G018137 and by the Defense Threat Reduction Agency.

REFERENCES

(1) Eddaoudi, M.; Moler, D. B.; Li, H.; Chen, B.; Reineke, T. M.; O'Keeffe, M.; Yaghi, O. M. *Acc. Chem. Res.* **2001**, *34*, 319.
(2) Farha, O. K.; Yazaydin, A. O.; Eryazici, I.; Malliakas, C. D.; Hauser, B. G.; Kanatzidis, M. G.; Nguyen, S. T.; Snurr, R. Q.; Hupp, J. T. *Nature Chem.* **2010**, *2*, 944.
(3) Furukawa, H.; Ko, N.; Go, Y. B.; Aratani, N.; Choi, S. B.; Choi, E.; Yazaydin, A. O.; Snurr, R. Q.; O'Keeffe, M.; Kim, J.; Yaghi, O. M. *Science* **2010**, *329*, 424.
(4) Rowsell, J. L. C.; Yaghi, O. M. *J. Am. Chem. Soc.* **2006**, *128*, 1304.
(5) Rowsell, J. L. C.; Yaghi, O. M. *Angew. Chem., Int. Ed.* **2005**, *44*, 4670.
(6) Jung, D. H.; Kim, D.; Lee, T. B.; Choi, S. B.; Yoon, J. H.; Kim, J.; Choi, K.; Choi, S. H. *J. Phys. Chem. B* **2006**, *110*, 22987.
(7) Ma, S.; Sun, D.; Ambrogio, M.; Fillinger, J. A.; Parkin, S.; Zhou, H. C. *J. Am. Chem. Soc.* **2007**, *129*, 1858.
(8) Ryan, P.; Broadbelt, L. J.; Snurr, R. Q. *Chem. Commun.* **2008**, 4132.
(9) Han, S. S.; Mendoza-Cortes, J. L.; Goddard, W. A., III *Chem. Soc. Rev.* **2009**, *38*, 1460.
(10) Dinca, M.; Dailly, A.; Liu, Y.; Brown, C. M.; Neumann, D. A.; Long, J. R. *J. Am. Chem. Soc.* **2006**, *128*, 16876.
(11) Dinca, M.; Long, J. R. *Angew. Chem., Int. Ed.* **2008**, *47*, 6766.
(12) Chen, B.; Ockwig, N. W.; Millward, A. R.; Contreras, D. S.; Yaghi, O. M. *Angew. Chem., Int. Ed.* **2005**, *44*, 4745.
(13) Mulfort, K. L.; Farha, O. K.; Stern, C. L.; Sarjeant, A. A.; Hupp, J. T. *J. Am. Chem. Soc.* **2009**, *131*, 3866.
(14) Himsl, D.; Wallacher, D.; Hartmann, M. *Angew. Chem., Int. Ed.* **2009**, *48*, 4639.
(15) Burchell, T.; Rogers, M. *SAE Tech. Pap. Ser.* **2000**, 2000-01-2205.
(16) Ma, L.; Lee, J. Y.; Li, J.; Lin, W. *Inorg. Chem.* **2008**, *47*, 3955.
(17) Wang, X.-S.; Ma, S.; Rauch, K.; Simmons, J. M.; Yuan, D.; Wang, X.; Yildrim, T.; Cole, W. C.; Lopez, J. L.; Meijere, A. d.; Zhou, H.-C. *Chem. Mater.* **2008**, *20*, 3145.
(18) U. S. Department of Energy. Energy Efficiency and Renewable Energy. http://www.eere.energy.gov/hydrogenandfuelcells/pdfs/free- domcar_targets_and_explanations.pdf, January 4, 2010 (accessed July 26, 2010).
(19) Getman, R. B.; Miller, J. H.; Wang, K.; Snurr, R. Q. *J. Phys. Chem. C* **2011**, *115*, 2066.
(20) Han, S. S.; Goddard, W. A., III *J. Am. Chem. Soc.* **2007**, *129*, 8422.
(21) Pässler, P.; Hefner, W.; Buckl, K.; Meinass, H.; Meiswinkel, A.; Wernicke, H.-J.; Ebersberg, G.; Müller, R.; Bässler, J.; Behringer, H.; Mayer, D. *Acetylene*; Wiley-VCH Verlag GmbH & Co. KGaA: New York, 2000.
(22) Düren, T.; Bae, Y.-S.; Snurr, R. Q. *Chem. Soc. Rev.* **2009**, *38*, 1237.
(23) Snurr, R. Q.; Yazaydin, A. O.; Dubbeldam, D.; Frost, H. In *Metal-Organic Frameworks: Design and Application*; MacGillivray, L. R., Ed.; John Wiley & Sons, Inc.: Hoboken, NJ, 2010.
(24) Han, S. S.; Choi, S. H.; Goddard, W. A., III *J. Phys. Chem. C* **2010**, *114*, 12039.
(25) Keskin, S.; Liu, J.; Rankin, R. B.; Johnson, J. K.; Sholl, D. S. *Ind. Eng. Chem. Res.* **2009**, *48*, 2355.
(26) Tafipolsky, M.; Amirjalayer, S.; Schmid, R. *Microporous Mesoporous Mater.* **2010**, *129*, 304.
(27) Martin, M. G.; Siepmann, J. I. *J. Phys. Chem. B* **1998**, *102*, 2569.
(28) Morse, P. M. *Phys. Rev.* **1929**, *34*, 57.
(29) Lennard-Jones, J. E. *Proc. Phys. Soc.* **1931**, *43*, 461.
(30) Allinger, N. L. *J. Am. Chem. Soc.* **1977**, *99*, 8127.
(31) Clark, M.; Cramer, R. D.; Van Opdenbosch, N. *J. Comput. Chem.* **1989**, *10*, 982.
(32) Brooks, B. R.; Bruccoleri, R. E.; Olafson, B. D.; States, D. J.; Swaminathan, S.; Karplus, M. *J. Comput. Chem.* **1983**, *4*, 187.
(33) Lin, H.; Truhlar, D. G. *Theor. Chem. Acc.* **2006**, *117*, 185.
(34) Duin, A. C. T. v.; Dasgupta, S.; Lorant, F.; Goddard, W. A., III *J. Phys. Chem. A* **2001**, *105*, 9396.
(35) Darkrim, F.; Levesque, D. *J. Chem. Phys.* **1998**, *109*, 4981.
(36) Breneman, C.; Wiberg, K. B. *J. Comput. Chem.* **1990**, *11*, 361.
(37) Xu, Q.; Zhong, C. *J. Phys. Chem. C* **2010**, *114*, 5035.
(38) Wilmer, C. E.; Snurr, R. Q. *Chem. Eng. J.* **2011**, *171*, 775.
(39) Rappé, A. K.; Casewit, C. J.; Colwell, K. S.; Goddard, W. A., III; Skiff, W. M. *J. Am. Chem. Soc.* **1992**, *114*, 10024.
(40) Michels, A.; Degraaff, W.; Tenseldam, C. A. *Physica* **1960**, *26*, 393.
(41) Jorgensen, W. L.; Maxwell, D. S.; TiradoRives, J. *J. Am. Chem. Soc.* **1996**, *118*, 11225.
(42) Jorgensen, W. L.; Madura, J. D.; Swenson, C. J. *J. Am. Chem. Soc.* **1984**, *106*, 6638.
(43) Martin, M. G.; Siepmann, J. I. *J. Phys. Chem. B* **1999**, *103*, 4508.
(44) Mayo, S. L.; Olafson, B. D.; Goddard, W. A., III *J. Phys. Chem.* **1990**, *94*, 8897.
(45) Williams, D. E.; Cox, S. R. *Acta Crystallogr., Sect. B: Struct. Sci.* **1984**, *40*, 404.
(46) Allen, M. P.; Tildesley, D. J. *Computer Simulation of Liquids*; Clarendon Press: Oxford, U.K., 1987.
(47) Hart, J. R.; Rappé, A. K. *J. Chem. Phys.* **1992**, *97*, 1109.
(48) Abraham, R. J.; Stolevik, R. *Chem. Phys. Lett.* **1978**, *58*, 622.
(49) Deng, W.-Q.; Xu, X.; Goddard, W. A., III *Phys. Rev. Lett.* **2004**, *92*, 166103.
(50) Li, A.; Lu, R.-F.; Wang, Y.; Wang, X.; Han, K.-L.; Deng, W.-Q. *Angew. Chem., Int. Ed.* **2010**, *49*, 3330.
(51) Han, S. S.; Deng, W. Q.; Goddard, W. A., III *Angew. Chem., Int. Ed.* **2007**, *46*, 6289.
(52) Garberoglio, G.; Skoulidas, A. I.; Johnson, J. K. *J. Phys. Chem. B* **2005**, *109*, 13094.
(53) Wang, Q.; Johnson, J. K.; Broughton, J. Q. *J. Chem. Phys.* **1997**, *107*, 5108.
(54) Feynman, R. P.; Hibbs, A. R. *Quantum Mechanics and Path Integrals*; McGraw-Hill: New York, 1965.
(55) Krishna, R.; van Baten, J. M. *Microporous Mesoporous Mater.* **2011**, *137*, 83.
(56) Kumar, A. V. A.; Jobic, H.; Bhatia, S. K. *J. Phys. Chem. B* **2006**, *110*, 16666.
(57) Leach, A. R. *Molecular Modelling*, 1st ed.; Longman: Englewood Cliffs, NJ, 2001.
(58) McQuarrie, D. A. *Statistical Mechanics*; University Science Books: Sausalito, CA, 2000.
(59) Frenkel, D. In *Computational Soft Matter: From Synthetic Polymers to Proteins, Lecture Notes*; Attig, N., Binder, K., Grubmuller, H., Kremer, K., Eds.; John von Neumann Institute for Computig: Julich, Germany, 2004; Vol. 23.
(60) Weigend, F.; Haser, M.; Patzelt, H.; Ahlrichs, R. *Chem. Phys. Lett.* **1998**, *294*, 143.
(61) Cramer, C. J. *Essentials of Computational Chemistry: Theories and Models*, 2nd ed.; John Wiley & Sons, Ltd: West Sussex, England, 2007.
(62) Lilienfeld, O. A. v.; Tkatchenko, A. *J. Chem. Phys.* **2010**, *132*, 234109.

(63) Grimme, S. *J. Chem. Phys.* **2003**, *118*, 9095.
(64) Boys, S. F.; Bernardi, F. *Mol. Phys.* **2002**, *100*, 65.
(65) Düren, T.; Sarkisov, L.; Yaghi, O. M.; Snurr, R. Q. *Langmuir* **2004**, *20*, 2683.
(66) Ma, S.; Sun, D.; Simmons, J. M.; Collier, C. D.; Yuan, D.; Zhou, H.-C. *J. Am. Chem. Soc.* **2008**, *130*, 1012.
(67) Düren, T.; Snurr, R. Q. *J. Phys. Chem. B* **2004**, *108*, 15703.
(68) Wang, S. Y. *Energy Fuels* **2007**, *21*, 953.
(69) Gallo, M.; Glossman-Mitnik, D. *J. Phys. Chem. C* **2009**, *113*, 6634.
(70) Cote, A. P.; Benin, A. I.; Ockwig, N. W.; O'Keeffe, M.; Matzger, A. J.; Yaghi, O. M. *Science* **2005**, *310*, 1166.
(71) El-Kaderi, H. M.; Hunt, J. R.; Mendoza-Cortes, J. L.; Cote, A. P.; Taylor, R. E.; O'Keeffe, M.; Yaghi, O. M. *Science* **2007**, *316*, 268.
(72) Garberoglio, G. *Langmuir* **2007**, *23*, 12154.
(73) Lan, J. H.; Cao, D. P.; Wang, W. C. *Langmuir* 2010, *26*, 220.
(74) Mendoza-Cortes, J. L.; Han, S. S.; Furukawa, H.; Yaghi, O. M.; Goddard, W. A. *J. Phys. Chem. A* 2010, *114*, 10824.
(75) Frost, H.; Düren, T.; Snurr, R. Q. *J. Phys. Chem. B* **2006**, *110*, 9565.
(76) Frost, H.; Snurr, R. Q. *J. Phys. Chem. C* **2007**, *111*, 18794.
(77) Park, K. S.; Ni, Z.; Cote, A. P.; Choi, J. Y.; Huang, R. D.; Uribe-Romo, F. J.; Chae, H. K.; O'Keeffe, M.; Yaghi, O. M. Proceedings of the National Academy of Sciences of the United States of America, 2006; Vol. *103*, p 10186.
(78) Hayashi, H.; Cote, A. P.; Furukawa, H.; O'Keeffe, M.; Yaghi, O. M. *Nat. Mater.* **2007**, *6*, 501.
(79) Banerjee, R.; Phan, A.; Wang, B.; Knobler, C.; Furukawa, H.; O'Keeffe, M.; Yaghi, O. M. *Science* **2008**, *319*, 939.
(80) Wang, B.; Cote, A. P.; Furukawa, H.; O'Keeffe, M.; Yaghi, O. M. *Nature* **2008**, *453*, 207.
(81) Murray, L. J.; Dinca, M.; Long, J. R. *Chem. Soc. Rev.* **2009**, *38*, 1294.
(82) Bhatia, S. K.; Myers, A. L. *Langmuir* **2006**, *22*, 1688.
(83) Garrone, E.; Bonelli, B.; Areán, C. O. *Chem. Phys. Lett.* **2008**, *456*, 68.
(84) Bae, Y.-S.; Snurr, R. Q. *Microporous Mesoporous Mater.* **2010**, *132*, 300.
(85) Yang, Q. Y.; Zhong, C. L. *J. Phys. Chem. B* **2006**, *110*, 17776.
(86) Yang, Q. Y.; Zhong, C. L. *ChemPhysChem* **2006**, *7*, 1417.
(87) Eddaoudi, M.; Kim, J.; Rosi, N.; Vodak, D.; Wachter, J.; O'Keeffe, M.; Yaghi, O. M. *Science* **2002**, *295*, 469.
(88) Wang, Q. M.; Shen, D. M.; Bulow, M.; Lau, M. L.; Deng, S. G.; Fitch, F. R.; Lemcoff, N. O.; Semanscin, J. *Microporous Mesoporous Mater.* **2002**, *55*, 217.
(89) Kondo, M.; Okubo, T.; Asami, A.; Noro, S.; Yoshitomi, T.; Kitagawa, S.; Ishii, T.; Matsuzaka, H.; Seki, K. *Angew. Chem., Int. Ed.* **1999**, *38*, 140.
(90) Noro, S.; Kitagawa, S.; Kondo, M.; Seki, K. *Angew. Chem., Int. Ed.* **2000**, *39*, 2081.
(91) Noro, S.; Kitaura, R.; Kondo, M.; Kitagawa, S.; Ishii, T.; Matsuzaka, H.; Yamashita, M. *J. Am. Chem. Soc.* **2002**, *124*, 2568.
(92) Furukawa, H.; Yaghi, O. M. *J. Am. Chem. Soc.* **2009**, *131*, 8875.
(93) Dybtsev, D. N.; Chun, H.; Yoon, S. H.; Kim, D.; Kim, K. *J. Am. Chem. Soc.* **2004**, *126*, 32.
(94) Bae, Y.-S.; Dubbeldam, D.; Nelson, A.; Walton, K. S.; Hupp, J. T.; Snurr, R. Q. *Chem. Mater.* **2009**, *21*, 4768.
(95) Yang, Q. Y.; Zhong, C. L. *J. Phys. Chem. B* **2005**, *109*, 11862.
(96) Jung, D. H.; Kim, D.; Lee, T. B.; Kim, J.; Choi, S. H. In *Advances in Nanomaterials and Processing, Pts 1 and 2*; Ahn, B. T., Jeon, H., Hur, B. Y., Kim, K., Park, J. W., Eds.; Trans Tech Publications Ltd.: Stafa-Zurich, Switzerland, 2007; Vol. 124−126.
(97) Sagara, T.; Klassen, J.; Ganz, E. *J. Chem. Phys.* **2004**, *121*, 12543.
(98) Yang, Q. Y.; Zhong, C. L. *J. Phys. Chem. B* **2006**, *110*, 655.
(99) Liu, J. C.; Culp, J. T.; Natesakhawat, S.; Bockrath, B. C.; Zande, B.; Sankar, S. G.; Garberoglio, G.; Johnson, J. K. *J. Phys. Chem. C* **2007**, *111*, 9305.
(100) Liu, J.; Lee, J. Y.; Pan, L.; Obermyer, R. T.; Simizu, S.; Zande, B.; Li, J.; Sankar, S. G.; Johnson, J. K. *J. Phys. Chem. C* **2008**, *112*, 2911.
(101) Han, S. S.; Deng, W. Q.; Goddard, W. A., III *Angew. Chem., Int. Ed.* **2007**, *46*, 6289.
(102) Yang, Q.; Zhong, C. *J. Phys. Chem. B* **2005**, *109*, 11862.
(103) Wong-Foy, A. G.; Matzger, A. J.; Yaghi, O. M. *J. Am. Chem. Soc.* **2006**, *128*, 3494.
(104) Panella, B.; Hirscher, M.; Putter, H.; Muller, U. *Adv. Funct. Mater.* **2006**, *16*, 520.
(105) Dailly, A.; Vajo, J. J.; Ahn, C. C. *J. Phys. Chem. B* **2006**, *110*, 1099.
(106) Kaye, S. S.; Dailly, A.; Yaghi, O. M.; Long, J. R. *J. Am. Chem. Soc.* **2007**, *129*, 14176.
(107) Buch, V. *J. Chem. Phys.* **1994**, *100*, 7610.
(108) Rowsell, J. L.; Millward, A. R.; Park, K. S.; Yaghi, O. M. *J. Am. Chem. Soc.* **2004**, *126*, 5666.
(109) Rowsell, J. L. C. Ph.D. Dissertation, University of Michigan, Ann Arbor, MI, 2005.
(110) Belof, J. L.; Stern, A. C.; Space, B. *J. Chem. Theory Comput.* **2008**, *4*, 1332.
(111) Basmadjian, D. *Can. J. Chem. Rev. Canadienne Chim.* **1960**, *38*, 141.
(112) Freeman, M. P. *J. Phys. Chem.* **1960**, *64*, 32.
(113) Feynman, R. P. *Rev. Mod. Phys.* **1948**, *20*, 367.
(114) Han, S. S.; Furukawa, H.; Yaghi, O. M.; Goddard, W. A., III *J. Am. Chem. Soc.* **2008**, *130*, 11580.
(115) Zhou, W.; Wu, H.; Hartman, M. R.; Yildirim, T. *J. Phys. Chem. C* **2007**, *111*, 16131.
(116) Xiang, S. C.; Zhou, W.; Zhang, Z. J.; Green, M. A.; Liu, Y.; Chen, B. L. *Angew. Chem., Int. Ed.* **2010**, *49*, 4615.
(117) Zhang, J. P.; Chen, X. M. *J. Am. Chem. Soc.* **2009**, *131*, 5516.
(118) Hu, Y. X.; Xiang, S. C.; Zhang, W. W.; Zhang, Z. X.; Wang, L.; Bai, J. F.; Chen, B. L. *Chem. Commun.* **2009**, 7551.
(119) Rosi, N.; Kim, J.; Eddaouddi, M.; Chen, B.; O'Keeffe, M.; Yaghi, O. M. *J. Am. Chem. Soc.* **2005**, *127*, 1504.
(120) Dietzel, P. D. C.; Besikiotis, V.; Blom, R. *J. Mater. Chem.* **2009**, *19*, 7362.
(121) Caskey, S. R.; Wong-Foy, A. G.; Matzger, A. J. *J. Am. Chem. Soc.* **2008**, *130*, 10870.
(122) Fischer, M.; Hoffmann, F.; Fröba, M. *ChemPhysChem* **2010**, *11*, 2220.
(123) Gautam, S.; Mitra, S.; Mukhopadhyay, R.; Chaplot, S. *Phys. Rev. E* **2006**, *74*, 041202.
(124) Dinca, M.; Long, J. R. *Angew. Chem., Int. Ed.* **2008**, *47*, 6766.
(125) Sun, Y. Y.; Kim, Y.-H.; Zhang, S. B. *J. Am. Chem. Soc.* **2007**, *129*, 12606.
(126) Zhou, W.; Yildirim, T. *J. Phys. Chem. C* **2008**, *112*, 8132.
(127) Lochan, R. C.; Khaliullin, R. Z.; Head-Gordon, M. *Inorg. Chem.* **2008**, *47*, 4032.
(128) Kosa, M.; Krack, M.; Cheetham, A. K.; Parrinello, M. *J. Phys. Chem. C* **2008**, *112*, 16171.
(129) Karra, J. R.; Walton, K. S. *Langmuir* **2008**, *24*, 8620.
(130) Kubas, G. J. *Metal Dihydrogen and s-bond Compleses—Structure, Theory, and Reactivity*; Kluwer Academic: New York, 2001.
(131) Kubas, G. J. *Acc. Chem. Res.* **1988**, *21*, 120.
(132) Wu, H.; Zhou, W.; Yildirim, T. *J. Am. Chem. Soc.* **2009**, *131*, 4995.
(133) Grajciar, L.; Bludsky, O.; Nachtigall, P. *J. Phys. Chem. Lett.* **2010**, *1*, 3354.
(134) Grimme, S. *J. Comput. Chem.* **2006**, *27*, 1787.
(135) Grimme, S.; Antony, J.; Ehrlich, S.; Krieg, H. *J. Chem. Phys.* **2010**, *132*, 154104.
(136) Williams, H. L.; Chabalowski, C. F. *J. Phys. Chem. A* **2001**, *105*, 646.
(137) Jansen, G.; Hesselmann, A. *J. Phys. Chem. A* **2001**, *105*, 11156.
(138) Rubes, M.; Kysilka, J.; Nachtigall, P.; Bludsky, O. *Phys. Chem. Chem. Phys.* **2010**, *12*, 6438.
(139) Zhao, Y.; Truhlar, D. G. *Theor. Chem. Acc.* **2008**, *119*, 525.
(140) Bludský, O.; Rubes, M.; Soldan, P.; Nachtigall, P. *J. Chem. Phys.* **2008**, *128*, 114102.

(141) Tafipolsky, M.; Amirjalayer, S.; Schmid, R. *J. Phys. Chem. C* **2010**, *114*, 14402.
(142) Mulfort, K. L.; Hupp, J. T. *J. Am. Chem. Soc.* **2007**, *129*, 9604.
(143) Mulfort, K. L.; Hupp, J. T. *Inorg. Chem.* **2008**, *47*, 7936.
(144) Mulfort, K. L.; Wilson, T. M.; Wasielewski, M. R.; Hupp, J. T. *Langmuir* **2009**, *25*, 503.
(145) Blomqvist, A.; Araujo, C. M.; Srepusharawoot, P.; Ahuja, R. *Proc. Natl. Acad. Sci. U. S. A.* **2007**, *104*, 20173.
(146) Sun, Q.; Jena, P.; Wang, Q.; Marquez, M. *J. Am. Chem. Soc.* **2006**, *128*, 9741.
(147) Yildirim, T.; Ciraci, S. *Phys. Rev. Lett.* **2005**, *94*, 175501.
(148) Sun, Q.; Wang, Q.; Jena, P.; Kawazoe, Y. *J. Am. Chem. Soc.* **2005**, *127*, 14582.
(149) Wang, Q.; Sun, Q.; Jena, P.; Kawazoe, Y. *J. Chem. Theory Comput.* **2009**, *5*, 374.
(150) Krasnov, P. O.; Ding, F.; Singh, A. K.; Yakobson, B. I. *J. Phys. Chem. C* **2007**, *111*, 17977.
(151) Hoang, T. K. A.; Antonelli, D. M. *Adv. Mater.* **2009**, *21*, 1787.
(152) Li, M.; Li, Y.; Zhou, Z.; Shen, P.; Chen, Z. *Nano Lett.* **2009**, *9*, 1944.
(153) Chandrakumar, K. R. S.; Ghosh, S. *Nano Lett.* **2008**, *8*, 13.
(154) Froudakis, G. E. *Nano Lett.* **2001**, *1*, 531.
(155) Wu, X.; Gao, Y.; Zeng, X. C. *J. Phys. Chem. C* **2008**, *112*, 8458.
(156) Kolmann, S. J.; Chan, B.; Jordan, M. J. T. *Chem. Phys. Lett.* **2008**, *467*, 126.
(157) Dalach, P.; Frost, H.; Snurr, R. Q.; Ellis, D. E. *J. Phys. Chem. C* **2008**, *112*, 9278.
(158) Sun, Y.; Ben, T.; Wang, L.; Qiu, S.; Sun, H. *J. Phys. Chem. Lett.* **2010**, *1*, 2753.
(159) Roussel, T.; Bichara, C.; Gubbins, K. E.; Pellenq, R. J.-M. *J. Chem. Phys.* **2009**, *130*, 174717.
(160) Venkataramanan, N. S.; Sahara, R.; Mizuseki, H.; Kawazoe, Y. *Int. J. Mol. Sci.* **2009**, *10*, 1601.
(161) Cao, D.; Lan, J.; Wang, W.; Smit, B. *Angew. Chem., Int. Ed.* **2009**, *48*, 4730.
(162) Tylianakis, E.; Klontzas, E.; Froudakis, G. E. *Nanotechnology* **2009**, *20*, 204030.
(163) Mavrandonakis, A.; Tylianakis, E.; Stubos, A. K.; Froudakis, G. E. *J. Phys. Chem. C* **2008**, *112*, 7290.
(164) Mavrandonakis, A.; Klontzas, E.; Tylianakis, E.; Froudakis, G. E. *J. Am. Chem. Soc.* **2009**, *131*, 13414.
(165) Goddard, W. A., III; Han, S. S. Patent AB01J2022FI, 2009.
(166) Klontzas, E.; Mavrandonakis, A.; Tylianakis, E.; Froudakis, G. E. *Nano Lett.* **2008**, *8*, 1572.
(167) Klontzas, E.; Tylianakis, E.; Froudakis, G. E. *J. Phys. Chem. C* **2009**, *113*, 21253.
(168) Muto, Y. *J. Phys. Math. Soc. Japan* **1943**, *17*, 629.
(169) Axilrod, B. M.; Teller, E. *J. Chem. Phys.* **1943**, *11*, 299.
(170) Sillar, K.; Hoffman, A.; Sauer, J. *J. Am. Chem. Soc.* **2009**, *131*, 4143.
(171) Svelle, S.; Tuma, C.; Rozanska, X.; Kerber, T.; Sauer, J. *J. Am. Chem. Soc.* **2009**, *131*, 816.
(172) Tuma, C.; Sauer, J. *Chem. Phys. Lett.* **2004**, *387*, 388.
(173) Tuma, C.; Sauer, J. *Phys. Chem. Chem. Phys.* **2006**, *8*, 3955.
(174) Ruthven, D. M. *Principles of Adsorption and Adsorption Processes*; John Wiley & Sons: New York, 1984.
(175) Peng, Q.; Chen, G.; Mizuseki, H.; Kawazoe, Y. *J. Chem. Phys.* **2009**, *131*, 214505.
(176) Gavezzotti, A. *J. Phys. Chem. B* **2003**, *107*, 2344.
(177) Belof, J. L.; Stern, A. C.; Eddaoudi, M.; Space, B. *J. Am. Chem. Soc.* **2007**, *129*, 15202.
(178) Vlugt, T. J. H.; Schenk, M. *J. Phys. Chem. B* **2002**, *106*, 12757.
(179) Garcia-Sanchez, A.; Dubbeldam, D.; Calero, S. *J. Phys. Chem. C* **2010**, *114*, 15068.
(180) Barthelet, K.; Marrot, J.; Riou, D.; Férey, G. *Angew. Chem., Int. Ed.* **2002**, *41*, 281.
(181) Serre, C.; Millange, F.; Thouvenot, C.; Nogues, M.; Marsolier, G.; Louer, D.; Férey, G. *J. Am. Chem. Soc.* **2002**, *124*, 13519.
(182) Férey, G.; Serre, C. *Chem. Soc. Rev.* **2009**, *38*, 1380.
(183) Coudert, F.-X.; Mellot-Draznieks, C.; Fuchs, A. H.; Boutin, A. *J. Am. Chem. Soc.* **2009**, *131*, 11329.
(184) Neimark, A. V.; Coudert, F.-X.; Boutin, A.; Fuchs, A. H. *J. Phys. Chem. Lett.* **2010**, *1*, 445.
(185) Zang, J.; Nair, S.; Sholl, D. S. *J. Chem. Phys.* **2011**, *134*, 184103.
(186) Boutin, A.; Springuel-Huet, M.; Nossov, A.; Gedeon, A.; Loiseau, T.; Volkringer, C.; Férey, G.; Coudert, F.; Fuchs, A. H. *Angew. Chem., Int. Ed.* **2009**, *48*, 8314.
(187) Tafilpolsky, M.; Amirjalayer, S.; Schmid, R. *Microporous Mesoporous Mater.* **2009**, *129*, 304.
(188) Dubbeldam, D.; Walton, K. S.; Ellis, D. E.; Snurr, R. Q. *Angew. Chem.* **2007**, *119*, 4580.
(189) Salles, F.; Ghoufi, A.; Maurin, G.; Bell, R. G.; Mellot-Draznieks, C.; Férey, G. *Angew. Chem., Int. Ed.* **2008**, *47*, 8487.
(190) Dubbeldam, D.; Krishna, R.; Snurr, R. Q. *J. Phys. Chem. C* **2009**, *113*, 19317.
(191) Vuong, T.; Monson, P. A. *Langmuir* **1996**, *12*, 5425.
(192) Fuchs, A. H.; Cheetham, A. K. *J. Phys. Chem. B* **2001**, *105*, 7375.
(193) Sircar *J. Chem. Soc., Faraday Trans. 1* **1985**, *81*, 1527.
(194) June, R. L.; Bell, A. T.; Theodorou, D. N. *J. Phys. Chem.* **1990**, *94*, 1508.
(195) Heuchel, M.; Snurr, R. Q.; Buss, E. *Langmuir* **1997**, *13*, 6795.
(196) Snurr, R. Q.; Bell, A. T.; Theodorou, D. N. *J. Phys. Chem.* **1993**, *97*, 13742.
(197) Smit, B.; Siepmann, J. I. *J. Phys. Chem.* **1994**, *98*, 8442.
(198) Vlugt, T. J. H.; Garcia-Perez, E.; Dubbeldam, D.; Ban, S.; Calero, S. *J. Chem. Theory Comput.* **2008**, *4*, 1107.
(199) Karavias, F.; Myers, A. L. *Langmuir* **1991**, *7*, 3118.
(200) Sandler, S. I. *Chemical, Biochemical, and Engineering Thermodynamics*; John Wiley and Sons, Inc.: New York, 2006.
(201) Dubbeldam, D., Ph.D Dissertation, Van't Hoff Institute for Molecular Sciences, University of Amsterdam, Amsterdam, The Netherlands, 2005.
(202) Jiang, S. Y.; Gubbins, K. E.; Zollweg, J. A. *Mol. Phys.* **1993**, *80*, 103.
(203) Haldoupis, E.; Nair, S.; Sholl, D. S. *J. Am. Chem. Soc.* **2010**, *132*, 7528.
(204) Keskin, S.; Sholl, D. S. *J. Phys. Chem. C* **2007**, *111*, 14055.
(205) Greathouse, J. A.; Ockwig, N. W.; Criscenti, L. J.; Guilinger, T. R.; Pohl, P.; Allendorf, M. D. *Phys. Chem. Chem. Phys.* **2010**, *12*, 12621.